

DEACTIVATION OF PdNi CATALYST ON NANOPOROUS CARBON SUPPORT DERIVED
FROM CATTAIL LEAVES IN SYNTHESIS OF PARTIALLY HYDROGENATED BIODIESEL
(H-FAME)



A Thesis Submitted in Partial Fulfillment of the Requirements
for the Degree of Master of Engineering in Chemical Engineering

Department of Chemical Engineering

FACULTY OF ENGINEERING

Chulalongkorn University

Academic Year 2020

Copyright of Chulalongkorn University

การเสื่อมสภาพของตัวเร่งปฏิกิริยาแพลเลเดียมนิกเกิลบนตัวรองรับคาร์บอนจากไบโธปฤยี
ในการสังเคราะห์ไบโอดีเซลที่ผ่านกระบวนการไฮโดรจีเนชันบางส่วน



วิทยานิพนธ์นี้เป็นส่วนหนึ่งของการศึกษาตามหลักสูตรปริญญาวิศวกรรมศาสตรมหาบัณฑิต
สาขาวิชาวิศวกรรมเคมี ภาควิชาวิศวกรรมเคมี
คณะวิศวกรรมศาสตร์ จุฬาลงกรณ์มหาวิทยาลัย
ปีการศึกษา 2563
ลิขสิทธิ์ของจุฬาลงกรณ์มหาวิทยาลัย

Thesis Title	DEACTIVATION OF PdNi CATALYST ON NANOPOROUS CARBON SUPPORT DERIVED FROM CATTAIL LEAVES IN SYNTHESIS OF PARTIALLY HYDROGENATED BIODIESEL(H-FAME)
By	Mr. Tripob Longprang
Field of Study	Chemical Engineering
Thesis Advisor	Professor SUTTICHAJ ASSABUMRUNGRAT
Thesis Co Advisor	Dr. Nuwong Chollacoop Associate Professor APILUCK EIAD-UA

Accepted by the FACULTY OF ENGINEERING, Chulalongkorn University in
Partial Fulfillment of the Requirement for the Master of Engineering

----- Dean of the FACULTY OF
ENGINEERING
(Professor SUPOT TEACHAVORASINSKUN)

THESIS COMMITTEE

----- Chairman
(Dr. PHUET PRASERTCHAROENSUK)

----- Thesis Advisor
(Professor SUTTICHAJ ASSABUMRUNGRAT)

----- Thesis Co-Advisor
(Dr. Nuwong Chollacoop)

----- Thesis Co-Advisor
(Associate Professor APILUCK EIAD-UA)

----- Examiner
(Professor BUNJERD JONGSOMJIT)

----- External Examiner
(Associate Professor Worapon Kiatkittipong)

ไตรภพ หลงปรารค์ : การเสื่อมสภาพของตัวเร่งปฏิกิริยาแพลเลเดียมนิกเกิลบนตัวรองรับคาร์บอนจากไบรูปฤกษ์ในการสังเคราะห์ไบโอดีเซลที่ผ่านกระบวนการไฮโดรจิเนชันบางส่วน. (DEACTIVATION OF PdNi CATALYST ON NANOPOROUS CARBON SUPPORT DERIVED FROM CATTAIL LEAVES IN SYNTHESIS OF PARTIALLY HYDROGENATED BIODIESEL(H-FAME)) อ.ที่ปรึกษาหลัก : ศ. ดร.สุทธิชัย อัสสะบารุงรัตน์, อ.ที่ปรึกษาร่วม : ดร.นงศ์ ชลคุป,รศ. ดร.อภิรักษ์ณ เอียดเอื้อ

ในปัจจุบันไบโอดีเซลนับเป็นพลังงานทางเลือกชนิดหนึ่งที่ใช้ทดแทนเชื้อเพลิงฟอสซิลอย่างกว้างขวาง เนื่องจากมีค่าพลังงานที่สูงใกล้เคียงกับเชื้อเพลิงฟอสซิล แต่เนื่องจากสามารถทำปฏิกิริยากับอากาศได้ง่าย ในงานใช้งานจึงต้องนำมาผสมกับน้ำมันดีเซลเพื่อให้มีคุณลักษณะที่เหมาะสมและเพิ่มอายุการเก็บรักษา กระบวนการพาร์เซียลไฮโดรจิเนชันเป็นหนึ่งในกระบวนการที่ใช้เพิ่มคุณภาพของน้ำมันไบโอดีเซล ในงานวิจัยนี้ได้ทำการผลิตตัวรองรับถ่านกัมมันต์จากไบรูปฤกษ์ด้วยกระบวนการไฮโดรเทอร์มัลคาร์บอนไนเซชันและกระบวนการกระตุ้นทางเคมี ถ่านกัมมันต์ที่ได้มีพื้นที่ผิวสูง 2002 ตารางเมตรต่อกรัม ซึ่งได้จากกระบวนการกระตุ้นด้วยโพแทสเซียมไฮดรอกไซด์ที่มีความเข้มข้น 4 โมลาร์ ที่อุณหภูมิ 900 องศาเซลเซียส งานวิจัยนี้ทำการศึกษาเงื่อนไขการทำปฏิกิริยาที่เหมาะสมและการลดลงของประสิทธิภาพของตัวเร่งปฏิกิริยาแบบไบเมทัลลิกแพลเลเดียมนิกเกิลในปฏิกิริยาพาร์เซียลไฮโดรจิเนชันที่สภาวะเงื่อนไขการทำปฏิกิริยาต่าง ๆ ไม่ว่าจะเป็นอุณหภูมิ (80, 100, 120 และ 140 องศาเซลเซียส), ความดัน (3, 4 และ 5 บาร์) และ ความเร็วรอบในการปั่นกวน (150, 200 และ 300 รอบต่อนาที) ซึ่งพบว่า ที่อุณหภูมิ 100 องศาเซลเซียส ที่ความดัน 4 บาร์ โดยมีความเร็วรอบในการปั่นกวนที่ 150 รอบต่อนาที เป็นสภาวะการทำปฏิกิริยาที่เหมาะสมซึ่งทำให้น้ำมันไบโอดีเซลทนต่อปฏิกิริยาการออกซิเดชันเพิ่มขึ้นมากถึง 18.34 ชั่วโมง และปัจจัยที่ทำให้เกิดการลดลงของประสิทธิภาพในการทำปฏิกิริยามาจากสองปัจจัยหลัก ได้แก่ การเกิดการจับตัวของโมเลกุลซัลเฟอร์จากน้ำมันไบโอดีเซลและคาร์บอนบนพื้นผิวดังกล่าว ซึ่งการเติมนิกเกิลในรูปแบบของไบเมทัลลิกสามารถช่วยเพิ่มการเกิดการเพิ่มซีสไอโซเมอร์และลดการถดถอยของประสิทธิภาพของตัวเร่งปฏิกิริยาในกระบวนการพาร์เซียลไฮโดรจิเนชัน

สาขาวิชา วิศวกรรมเคมี

ปีการศึกษา 2563

ลายมือชื่อนิสิต

ลายมือชื่อ อ.ที่ปรึกษาหลัก

ลายมือชื่อ อ.ที่ปรึกษาร่วม

ลายมือชื่อ อ.ที่ปรึกษาร่วม

6270097821 : MAJOR CHEMICAL ENGINEERING

KEYWORD:

Tripob Longprang : DEACTIVATION OF PdNi CATALYST ON NANOPOROUS CARBON SUPPORT DERIVED FROM CATTAIL LEAVES IN SYNTHESIS OF PARTIALLY HYDROGENATED BIODIESEL(H-FAME). Advisor: Prof. SUTTICHA ASSABUMRUNGRAT Co-advisor: Dr. Nuwong Chollacoop, Assoc. Prof. APILUCK EIAD-UA

Nowadays, biodiesel is an alternative energy that is widely used to replace fossil fuels because of its high heat value comparable to fossil fuels. Biodiesel was easily oxidized within air. It is commonly blended with diesel fuel to have the proper properties and increase shelf life. Partial hydrogenation is one of the processes used to enhance the properties of biodiesel. In this research, bimetallic PdNi on nanoporous carbon (NPC) support derived from cattail leaves was successfully synthesized via hydrothermal carbonization and chemical activation. The prepared nanoporous carbon has a high surface area of $2002 \text{ m}^2\text{g}^{-1}$, obtained by activation process with 4 M of potassium hydroxide at $900 \text{ }^\circ\text{C}$. Optimal condition and deactivation of PdNi/NPC in partial hydrogenation at various temperatures (80, 100, 120 and $140 \text{ }^\circ\text{C}$), pressure (3, 4 and 5 bar) and stirring rate (150, 200 and 300 rpm) were investigated. It was found that an operation at $100 \text{ }^\circ\text{C}$, 4 bar and a stirring speed of 150 rpm offered the biodiesel with increased oxidation stability to 18.34 h. Furthermore, the results indicated that the deactivation of catalyst occurred from two main factors: poisoning of sulfur molecules in biodiesel feedstock and carbon residue covering on the surface of the catalyst. The addition of nickel in the bimetallic form led to increased cis-C18:1 selectivity and decreased the catalyst deactivation in the partial hydrogenation process.

Field of Study: Chemical Engineering

Student's Signature

Academic Year: 2020

Advisor's Signature

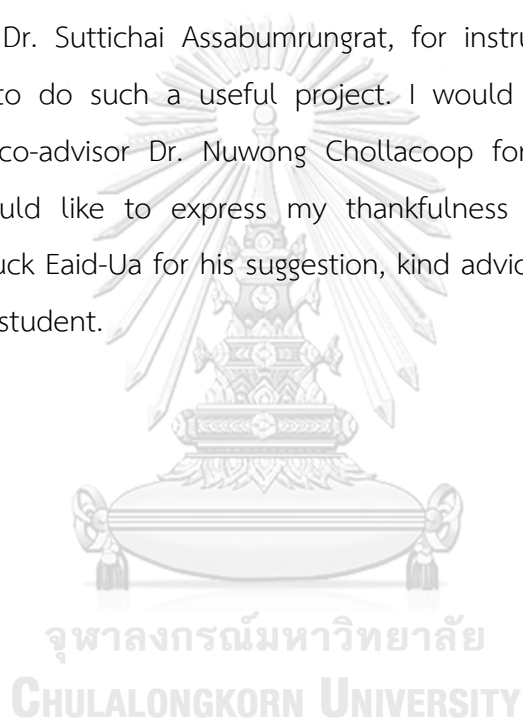
Co-advisor's Signature

Co-advisor's Signature

ACKNOWLEDGEMENTS

Firstly, I would like to thank the Department of Chemical Engineering, Chulalongkorn University, College of Nanotechnology, King Mongkut's Institute of Technology Ladkrabang, National Metal and Materials Technology Center (MTEC), Thailand Graduate Institute of Science and Technology (TGIST) for all the support to this research to be achieved.

Secondly, I would like to express my sincere gratefulness of gratitude to my advisor Professor Dr. Suttichai Assabumrungrat, for instruction, many supports, and instructional me to do such a useful project. I would like to express my special gratitude to my co-advisor Dr. Nuwong Chollacoop for suggestions, and valuable information. I would like to express my thankfulness to my co-advisor Assistant Professor. Dr. Apiluck Eaid-Ua for his suggestion, kind advice, and supports, since being an undergraduate student.



Tripob Longprang

TABLE OF CONTENTS

	Page
.....	iii
ABSTRACT (THAI)	iii
.....	iv
ABSTRACT (ENGLISH)	iv
ACKNOWLEDGEMENTS	v
TABLE OF CONTENTS	vi
CONTENT OF TABLES	x
CONTENT OF FIGURES	xi
CHAPTER 1	1
INTRODUCTION	1
1.1 Motivation	1
1.2 Research objective	3
1.3 Scope of works	3
1.4 Implementation plan	3
1.5 Expected output	4
CHAPTER 2	5
THEORY AND LITERATURE REVIEWS	5
2.1 Biomass	5
2.1.1 Biomass composition	5
2.2 Cattail leaves	10
2.2.1 Source of found	11

2.2.2 Characteristics of Narrowleaf cattail.....	11
2.2.3 Propagation	12
2.3 Hydrothermal process.....	12
2.3.1 Reaction mechanism	12
2.3.1.3 Decarboxylation.....	13
2.3.1.4 Polymerization	13
2.3.1.5 Condensation	13
2.3.1.6 Aromatization	13
2.4 Carbonization process.....	13
2.5 Pore activation	14
2.5.1 Physical activation.....	14
2.5.2 Chemical activation.....	15
2.6 Biodiesel	16
2.6.1 Synthesis of biodiesel.....	16
2.6.2 Biodiesel properties	17
2.7 Hydrogenation of unsaturated FAME	19
2.8 Catalyst for hydrogenation.....	20
2.8.1 Homogeneous catalyst.....	20
2.8.2 Heterogeneous catalyst	21
2.9 Preparation of catalysts on support.....	22
2.9.1 Co-precipitation method	23
2.9.2 Adsorption	23
2.9.3 Ion exchange.....	24
2.9.4 Impregnation.....	24

2.10 Catalyst deactivation in partial hydrogenation of biodiesel.....	25
2.11 Pore characteristic of porous materials.....	25
2.11.1 Classification of porous materials.....	25
2.11.2 Adsorption isotherm.....	25
2.12 Literature review.....	28
CHAPTER 3.....	35
RESEARCH METHODOLOGY.....	35
3.1 Nanoporous carbon preparation.....	36
3.2 Characterization of nanoporous carbon.....	36
3.3 Catalyst preparation.....	38
3.4 Catalyst characterization.....	39
3.5 Partial hydrogenation of palm biodiesel.....	40
3.6 Biodiesel analysis.....	40
CHAPTER 4.....	42
RESULTS AND DISCUSSION.....	42
4.1 Characteristics of cattail leaves-derived nanoporous carbon.....	42
4.2 Catalytic activity in partial hydrogenation of palm H-FAME.....	51
4.2.1 Effect of reaction temperature.....	51
4.2.2 Effect of reaction pressure.....	53
4.2.3 Effect of catalyst type (monometallic and bimetallic catalysts).....	55
4.3 Deactivation of catalysts in partial hydrogenation.....	57
4.3.1 Effect of reaction temperature.....	57
4.3.2 Effect of reaction pressure.....	59
4.3.3 Effect of stirring rate.....	61

4.3.4 Catalyst stability.....	62
CHAPTER 5.....	64
CONCLUSIONS.....	64
5.1 Conclusions.....	64
5.2 Recommendations.....	65
APPENDIX.....	67
APPENDIX A.....	68
RAW MATERIAL DATA.....	68
A.1 Specification data of palm biodiesel (B100).....	68
APPENDIX B.....	69
BASIC CALCULATION.....	69
B.1 Poly-FAME (C18:2 and C18:3) conversion.....	69
B.2 Calculation of volume of H ₂ adsorption on catalyst.....	69
B.3 Calculation of metal active sites.....	69
B.4 Calculation of metal dispersion.....	69
REFERENCES.....	71
VITA.....	79

CONTENT OF TABLES

Table 1.1 Implementation plan.....	4
Table 2.1 The composition of lignocellulose in biomass.....	8
Table 2.2 Identification of cattail plant.....	10
Table 2.3 Effect of activation condition and physical properties of activated carbon	29
Table 2.4 FAME compositions, TOFs, and ratio of trans/cis C18:1 of Pd/MCM-41-SiO ₂ and Pd/MCM-41-silatrane.....	30
Table 4.1 Function groups of the CLs, CLs hydrochar, CLs derived NPC and PdNi/NPC	44
Table 4.2 Proximate and ultimate analysis of cattail leaves (CLs).....	45
Table 4.3 Textural properties of CLs derived NPC, Pd/NPC, Ni/NPC and PdNi/NPC..	49
Table 4.4 Effect of temperature to FAME compositions and biodiesel properties of palm BDF and H-FAME over Pd/NPC, Ni/NPC and PdNi/NPC at reaction time of 4 h.	51
Table 4.5 Effect of pressure to FAME compositions and biodiesel properties of palm BDF and H-FAME over Pd/NPC, Ni/NPC and PdNi/NPC at reaction time of 4 h.....	53
Table 4.6 FAME compositions and biodiesel properties of palm BDF and H-FAME over Pd/NPC, Ni/NPC and PdNi/NPC at reaction time of 4 h.....	56
Table 4.7 BET surface area and metal dispersion at varied temperature.....	59
Table 4.8 BET surface area and metal dispersion at varied pressure.....	60
Table 4.9 BET surface area and metal dispersion at varied stir rate.....	61
Table A.1 Specification of palm biodiesel (Fatty Acid Methyl Ester: FAME) B100....	68

CONTENT OF FIGURES

Figure 2.1 Chemical structure of cellulose.....	6
Figure 2.2 Chemical structure of hemicellulose.....	7
Figure 2.3 Chemical structure of lignin.....	8
Figure 2.4 Characteristic of cattail plant.....	10
Figure 2.5 Overall reaction of methyl ester formation in transesterification.....	17
Figure 2.6 Hydrogenation of polyunsaturated FAME.....	20
Figure 2.7 IUPAC classification: Physisorption isotherm type.....	26
Figure 2.8 Composition of biodiesel feed and H-FAME derived from batch (B) and continuous-flow (C) reactors at different conversions of C18:2 and C18:3.....	31
Figure 3.1 Schematic diagram of research methodology.....	35
Figure 3.2 Schematic diagram of Horizontal tube furnace for chemical activation of cattail leave to produce nanoporous	36
Figure 4.1 CLs derived NPC synthesis process effect on yield.....	42
Figure 4.2 Fourier transform infrared spectroscopy (FTIR) spectra of CLs derived NPC and post-loaded catalyst.....	43
Figure 4.3 Scanning electron microscope (SEM) micrographs of (a) CLs, (b) CLs hydrochar, (c) CLs derived NPC at 500x and (d) 2000x magnification.....	46
Figure 4.4 Energy dispersed X-ray (EDX) spectra of PdNi/NPC.....	47
Figure 4.5 TEM micrograph of the NPC, Pd/NPC, Ni/NPC and PdNi/NPC catalysts.....	48
Figure 4.6 (a) N ₂ adsorption and desorption isotherms and (b) pore size distribution of NPC, Pd/NPC, Ni/NPC and PdNi/NPC.....	49
Figure 4.7 XRD pattern of the NPC, Pd/NPC, Ni/NPC and PdNi/NPC catalysts.....	50

Figure 4.8 Effect of temperature on C18 composition.....	52
Figure 4.9 Effect of temperature on cis/trans-isomer of C18:1 composition.....	52
Figure 4.10 Effect of operating pressure on C18 composition.....	54
Figure 4.11 Effect of operating pressure on cis/trans-isomer of C18:1 composition.....	54
Figure 4.12 Effect of monometallic and bimetallic of PdNi on C18 composition.....	56
Figure 4.13 Effect of catalyst type on cis/trans-isomer of C18:1 composition.....	57
Figure 4.14 SEM images of PdNi/NPC catalyst (a) before and after partial hydrogenation at different temperature (b) 80 °C, (c) 100 °C, (d) 120 °C and (e) 140 °C	58
Figure 4.15 SEM images of PdNi/NPC catalyst (a) before and after partial hydrogenation at different temperature (b) 3 bar, (c) 4 bar and (d) 5 bar.....	60
Figure 4.16 SEM images of PdNi/NPC catalyst (a) before and after partial hydrogenation at different stir rate (b) 250 rpm, (c) 500 rpm and (d) 750 rpm.....	62
Figure 4.17 Catalytic stability of Pd/NPC and PdNi/NPC catalyst.....	63

CHAPTER 1

INTRODUCTION

1.1 Motivation

Economic and industrial development are growing extensively nowadays. These lead to progressive growth of energy consumption and depletion of unsustainable energy sources. Petroleum is one of the most widely used unsustainable source as feedstock for production of wide variety of fuels such as Gasoline, LPG, Jet fuel, Heavy fuel oil, Kerosene and especially diesel [1]. Diesel is the main power source of industrial and agricultural machinery including automotive which are the essential facilities in daily life [2, 3]. Biodiesel is one of the promising renewable energy to replace diesel fuel due to its equivalent high heating value of diesel, better engine lubrication and low environmental impact [2-4]. Biodiesel is commonly produced through the chemical reactions of transesterification and esterification by reacting triglyceride molecule with an alcohol (typically methanol) into fatty acid methyl esters (FAMES). Biodiesel synthesized from transesterification indicated the low fuel properties in terms of oxidation stability and cold flow properties compared with diesel [5, 6]. For this problem, blending a little amount of biodiesel with diesel has been used in the ratio of biodiesel to diesel at 10 percent (B10) and 20 percent (B20) up to the fuel properties of biodiesel [7].

Partial hydrogenation is a conventional method to improve fuel cold flow property and oxidation stability of biodiesel directly by adding hydrogen atoms at double and triple bonds (Polyunsaturated FAME (C18:2 and C18:3)) in hydrocarbon chains to maximize the monounsaturated FAME (C18:1) in hydrogenated biodiesel (H-FAME). Biodiesel H-FAME can use as standalone biodiesel except blending with diesel [8]. In this reaction, heterogeneous catalysts are preferred because of their potential low cost, required smaller amount of water for separation and catalysts cleaning that

affect to increasing in treatment system cost when compared with homogeneous catalyst [9, 10].

Noble transition metals such as palladium (Pd) and platinum (Pt) are usually applied as an active phase of heterogeneous catalyst in partial hydrogenation of FAMEs, which have a good catalytic activity at low temperature and pressure [11, 12]. Moreover, palladium has a good selectivity in cis-trans isomerization to promote the cis isomer of C18:1 structure that lead to increase cold flow property of biodiesel due to its crystallization point [13]. Although palladium (Pd) and platinum (Pt) have a good catalytic activity, in real production the amount of noble metal catalysts needs to be minimized due to their high cost. For solving this problem, transition metal catalysts such as nickel (Ni), cobalt (Co), magnesium (Mg), sodium (Na), calcium (Ca), Iron (Fe) and barium (Ba) have been selected for use instead due to their lower cost compared with commercial metal catalysts (Pd and Pt) and some addition properties such as exterminated of sulfur [11, 14]. Although the cost of transition metal catalysts is lower than palladium and platinum, they show much lower catalytic activity. For solving this problem, addition of some noble metals is still a common practice for increasing activity instead of standalone non noble metal catalysts. In recent years, bimetallic form have been researched and developed because of researchers need to use synergistic effect of bimetallic form to increase properties of catalysts such as catalyst lifetime, sulfur tolerance and dispersion of active metal for improving catalyst stability and preventing the deactivation of catalysts [15, 16]. So, deactivation of catalyst in production process is the main concern in industrial applications because it could affect the operating cost in term of shutdown of the production to change deactivated catalysts to fresh catalysts. Deactivation of catalysts occurs from many factors as operation conditions which have effect to catalysts directly, degradation of some components and contaminated elements (Sulfur content) in feedstock [17, 18].

In this research, it is interesting to synthesize catalysts in bimetallic form (PdNi) on high porosity of the activated carbon support by using cattail leave as raw material, to investigate the stability and deactivation of catalysts in a batch reactor and to find optimal conditions to prevent the catalysts deactivation.

1.2 Research objective

To synthesize NiPd catalyst in bimetallic form on nanoporous carbon support from cattail leave via Hydrothermal carbonization (HTC) process and to investigate the effects of temperature and pressure on deactivation of catalysts in partial hydrogenation reaction for improve the cold flow properties of palm biodiesel.

1.3 Scope of works

1.3.1 High porosity carbon support was prepared using cattail leaves as carbon source via hydrothermal carbonization method (HTC). Potassium hydroxide (KOH) has been used as an activating agent to promote porosity in mesoporous length (2-50 nm).

1.3.2 The catalysts were prepared by wet impregnation method using loading of 1%wt Pd and 10%wt Ni precursors on nanoporous carbon (NPC) support from cattail leave and catalysts calcination temperature at 400-600 °C

1.3.3 The catalytic activity of bimetallic PdNi/NPC was tested in partial hydrogenation of palm oil using a batch type reactor and compared with monometallic Pd/NPC and Ni/NPC catalysts.

1.3.4 The catalysts deactivation from the effects of operation temperature at 80-160 °C, pressure at 4-6 bar and mechanical damage occurred from stir rate was investigated as well as catalysts stability.

1.4 Implementation plan

There are 8 steps to conduct in this research work as shown in Table 1.1

1.4.1 Conduct literature survey and reviews

1.4.2 Carry out synthesis and characterization of catalysts

1.4.3 Prepare proposal examination

1.4.4 Improve biodiesel partial hydrogenation reaction

1.4.5 Study deactivation and stability of catalysts

1.4.6 Write thesis book and prepare thesis defending examination

Table 1.1 Implementation plan

Activity	2020												2021					
	1	2	3	4	5	6	7	8	9	10	11	12	1	2	3	4	5	6
Conduct literature survey and reviews	■	■	■	■	■	■	■	■	■	■	■	■	■	■	■	■		
Carry out synthesis and characterization of catalysts	■	■	■	■	■	■	■	■	■	■	■							
Prepare proposal examination								■	■	■	■	■						
Improve biodiesel partial hydrogenation reaction											■	■	■	■				
Studied deactivation and stability of catalysts														■	■	■		
Write thesis book and prepare thesis defending examination										■	■	■	■	■	■	■	■	■

1.5 Expected output

To obtain the optimal conditions for improvement of biodiesel fuel properties and catalysts deactivation prevention in addition with catalyst stability in partial hydrogenation reaction.

CHAPTER 2

THEORY AND LITERATURE REVIEWS

2.1 Biomass

Thailand is an agricultural country with many agricultural products such as rice, sugar, cassava, rubber, palm oil, etc. Biomass is a common organic substance from nature that non-toxic and biodegradable. Biomass stored energy within itself, this is because plants rely on sunlight and carbon dioxide for photosynthesis and growth. Solar energy is used as a power source for plants to synthesize starch and sugar and store them in different parts of the plant. Therefore, when used as a fuel, energy is obtained then converted to a solid-state in charcoal and can be utilized. Examples of these organic matters are grass waste, wood waste, agricultural waste, or some industrial waste such as sawdust, straw, rice husk, bagasse, etc [19].

2.1.1 Biomass composition

Biomass is a mixture of organic and small quantities of inorganic substances found. The main component of biomass is cellulose, hemicellulose, lignin, and extract which are the main components of lignocellulose material. The structure is mostly composed of sugars and sugar polymers (Polysaccharides). The amount of constituents in each type of biomass differs depending on the type of biomass, tissue type, And the growing conditions. Biomass contains high oxygen content compared to fossil fuels. Dry biomass typically contains 30-40% of oxygen, 30-60% of carbon, and 5-6% of hydrogen depending on the ash content, while nitrogen, sulfur, and chlorine contain less than 1% of biomass and can be found in the structure of some biomass. The biomass composition was reduced respectively as follows by carbon, oxygen, hydrogen, nitrogen, calcium, potassium, silicon, magnesium, and aluminum. Biomass inorganic compounds are found in ash. The portion of carbohydrate in biomass contains cellulose and hemicellulose While the non-carbohydrate portion

contains lignin. Cellulose and hemicellulose increase the structural and mechanical strength of plants, while non-carbohydrate lignin stabilizes these structures [20, 21].

2.1.1.1 Cellulose

Cellulose is the most abundant polymer in plant cells. It is an important part of the cell wall that responsible for strengthening the plant structure. Usually, cellulose is combined with lignin, hemicellulose, pentosan, gum, tannin, lipid, and coloring matter. Cellulose has a crystalline structure and resistant to acids and bases. Cellulose has a general molecular formula $(C_6H_{10}O_5)_n$ is a long-chain polysaccharide formed by the β -1,4 glycosidic of the D-glucopyranose with a high degree of polymerization (approximately 10,000) and a high molecular weight (approximately 500,000). Since the structure of the fibers is formed by hydrogen bonds. Cellulose is insoluble in water, organic matter, and solutions of weak bases or weak acids. But can be soluble in strong acids or strong bases and partially soluble in water at 302 °C and completely soluble at 330 °C under critical water conditions [21].

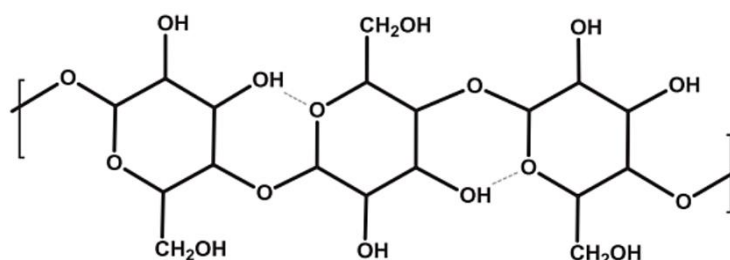


Figure 2.1 Chemical structure of cellulose

2.1.1.2 Hemicellulose

Hemicellulose occurs in approximately 20–30% of the biomass, which is an amorphous heteropolysaccharide that has a lower degree than cellulose and is easily reduced through heat treatment. It is formed by a high branched chain, a straight chain composed mainly of xylan and glucomannan. The structure of hemicellulose differs depending on the biomass source generally composed of D-glucopyranose, D-

galactopyranose, D-mannopyranose monomers, L-arabinofuranose, and D-xylopyranose. Hemicellulose monomers have sugar about 100-200 polymers per hemicellulose molecule. Usually, the hemicellulose content in wood is higher than the agricultural biomass [21].

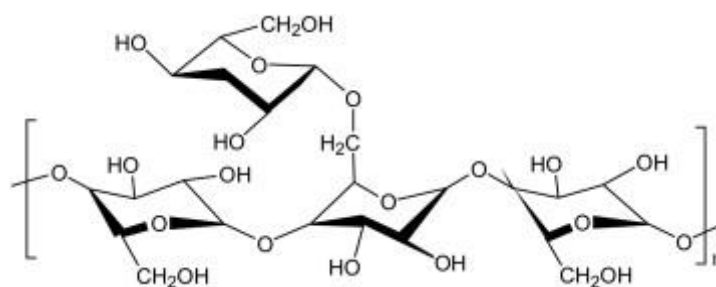


Figure 2.2 Chemical structure of hemicellulose

2.1.1.3 Lignin

Lignin is an important component of plant tissues to strengthen the plant cell wall, protect the structure, and stored energy. It is a complex natural polymer compound connected to a large amorphous structure that has hydrophobic properties. Lignins provide mechanical strength to plant structures through the connection between fibers (Reinforcing agent) with the cell wall, often in conjunction with cellulose and hemicellulose to form lignocellulose. Lignocellulose is mainly used as precursor to produce activated carbon. Lignocellulose composition in biomass show in **Table 2.1**. Lignin is aromatic compounds in phenylpropane with most hydroxyl and methyl groups linked by ether bonds. Lignin occurs in 18-25% hardwood and 25–35% softwood. Lignin in softwood biomass is composed of coniferyl alcohol while Lignin in solid wood composed of synthetic alcohol contains coniferyl alcohol and sinapyl alcohol as a monomer. Lignin does not decompose in both strong acids and bases. It is more resistant to natural degradation and biodegradation compared to other elements in plant structure because of its stabilization structure therefore, lignin gives biomass a higher calorific value. The lignin structure is extremely important for productivity during the hydrothermal

process because phenol compounds with ethyl and methyl groups are the main compounds produced by lignin degradation [21] [22].

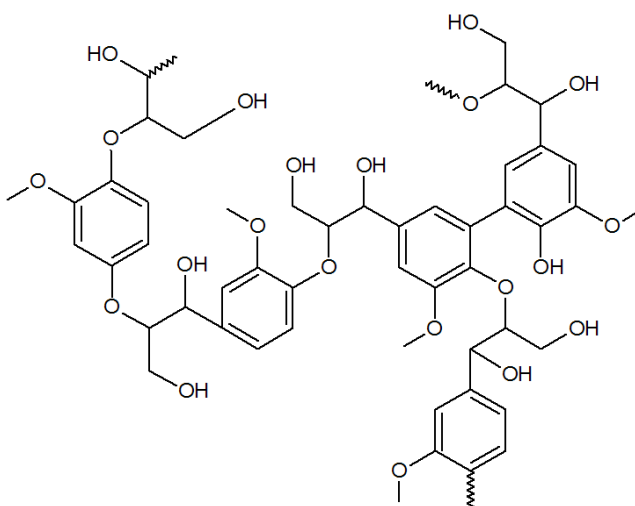


Figure 2.3 Chemical structure of lignin

Table 2.1 The composition of lignocellulose in biomass [22]

Biomass	Cellulose (%)	Hemicellulose (%)	Lignin (%)
Cattail leave	63	8.7	9.6
Rice straw	32-41	15-25	10-18
Hard wood	40-44	18-40	18-29
Bagasse	27-57	24-35	11-26
Coconut shell	30.63	26.83	33.35
Wheat straw	30	50	15

2.1.1.4 Extracts

Extracts are a group of chemical substance that can be extracted from biomass using polar and non-polar solvents. Extracts contains organic and inorganic compounds include proteins, fats, fatty acids, sugars, phenol terpene, acids, and resins. Types and quantities of these elements depending on the type of biomass typically weigh less than 2% of the weight of biomass. These extracts are essential to

establish plant characteristics such as color, flavor, and durability. Extracts can be classified by solute type as water, toluene, ether solvent according to the solvent used in the separation. Herbaceous plant such as soybean plants, corn, and sugarcane plants contain a high amount of extracts [21].

2.1.2 Quantitative composition

The Quantitative composition of biomass consists of moisture, ash, volatile matter, and fixed carbon [23].

2.1.2.1 Moisture

The moisture content in biomass is a very important property in the use of biomass as fuel. If biomass contains a large amount of moisture, the combustion efficiency is greatly reduced. The moisture content in biomass was determined by the lost weight after drying the biomass at 105–110 °C until the weight of the biomass remains constant. Water or moisture will evaporate from the biomass during drying. The moisture content in biomass depends on the type of biomass. The moisture content of wood biomass ranges from 25–65%, while in sludge biomass that found in industrials have moisture content is more than 90% [23].

2.1.2.2 Ash

The ash content in biomass is another important property in the use of biomass as fuel. If biomass has a high ash content, it will reduce the combustion efficiency. The ash content in biomass was determined by the remaining weight from the burning of biomass under the atmosphere at 575 °C for at least 3 hours. Organic components in the biomass were completely burned into carbon dioxide and water. While the inorganic components in biomass are oxidized to form an oxide compound (Ash) [23].

2.1.2.3 Volatile matter

The vapor content of biomass is the lost weight after heating the biomass under specified conditions, i.e. 900 °C for 7 minutes or until the weight stabilizes without exposed to air. Vapors are produced by thermal distillation or pyrolysis [23].

2.1.2.4 Fixed carbon

The fixed carbon content is a stable part of the biomass structure after heating biomass at 900 °C, which most contain carbon. The fixed carbon content is calculated from following equation [23].

$$\%FC = 100 - (\%M + \%A + \%VM)$$

When %FC: Fixed carbon

%M: Moisture

%A: Ash

%VM: Volatile matter

2.2 Cattail leaves

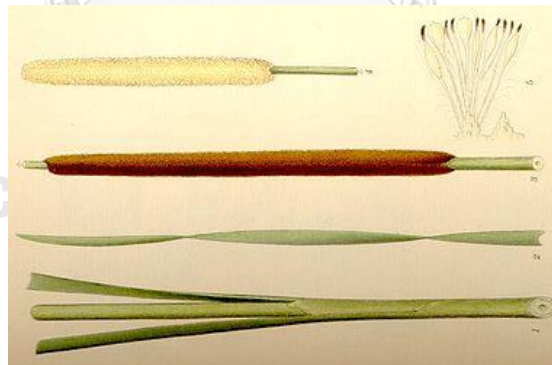


Figure 2.4 Characteristic of cattail plant

Table 2.2 Identification of cattail plant [24]

Identification	
Scientific name	<i>Typha angustifolia L.</i>
Common name	Cattail plant, Lesser bulrush, Narrowleaf cattail, lesser reedmace
Family	Typhaceae

Genus	Typha
Species	T. angustifolia

2.2.1 Source of found

They are distributed in Thailand throughout the region in both the freshwater and saltwater basins. It originated in Europe and America. Currently, there is a species spread throughout the world [24].

2.2.2 Characteristics of Narrowleaf cattail

2.2.2.1 The cattail leaves are softwood leaves split into panels into two sides. A single leaf plant, the base of the leaf is spread out into a thick sheath, covered with each other by the old leaves on the outside, and the young leaves on the inside. The inner leaf sheath looks like a long and sticky mucus. The leaves are flattened, 1.2-1.8 cm wide, 1-2 m long, from the cross-section. The upper leaf plate is slightly curved due to the spongy resilient cells in the middle of the leaf. The leaves below are flat. The structure of the cattail leaves consists of 38.5% cellulose fibers, 37.6% hemicellulose, 12.8% lignin, 11.1% ash, about 70-80% moisture content [24].

2.2.2.2 Cattail flowers are a discounted bouquet The shape is a brown cylinder. Many flowers are sticking together like a large incense. The peduncle is solid, with the same-sex stem. The solid peduncle is almost the same height as the dense, brown leaves. The flowers contain 40% fiber, 63% cellulose, 8.7% hemicellulose, 9.6% lignin, 2% ash, 1.4% wax, approximately 8.9% moisture [24].

Male flowers are loose clusters at the end of the inflorescence 15-30 cm long, with a bouquet diameter of approximately 0.2-0.7 cm, 1-3 bracts, 2-3 male flowers, and spoon-shaped hairs in 3 stacks [24].

Female flowers are at the bottom, small flowers packed. They are cylindrical, 5-30 cm long, and 2 cm in diameter. The ovary has long stems and many white hairs. Often separated from the male flower with the stem [24].

2.2.2.3 The fruit is small, falling off along the stem. Seeds hang down in streaks [24].

2.2.3 Propagation

Cattail has propagated by seeds. The seeds are silky and can be blow away with the wind. They are distributed throughout the world in tropical and temperate areas. For Thailand, it can be found in every region in the wetland area [24].

2.3 Hydrothermal process

The hydrothermal process is a chemical processing used to convert biomass into solid products or hydrothermal products (Hydrochar) via reaction under heat and pressure. Hydrothermal is an exothermic process that reduces the oxygen and hydrogen content of biomass raw materials by using water as a reagent to break down the bonding of carbohydrates because the biomass composition is less stable under water-saturated conditions. The temperature for use is between 140-220 °C in a sealed reactor and carbon-like material is obtained under mild hydrothermal synthesis conditions with short reaction times up to several hours (1-48 h) at a pressure of about 10 bar. Biomass degradation normally occurs at temperatures around 180 °C, where the intensity of the reaction is influenced by an increase of temperature and reaction time leading to a higher carbon product. Hydrothermal products are solids (Hydrochar), liquid and gas solutions (Approximately 10% by weight of raw materials). Characteristics of the resulting hydrochar have an increase of fixed carbon content, homogeneous, hydrophobic property [25-27].

2.3.1 Reaction mechanism

2.3.1.1 Hydrolysis

Hydrolysis is reaction to use water molecules (H_2O) to react with substances such as biomass, etc. The water molecules will break the bond of lignin, cellulose and hemicellulose which is a component in biomass from a long chain of bonds (Large molecules) will break into shorter chains or smaller molecules [27].

2.3.1.2 Hydration

Hydration is the reaction to removal of water molecules (H_2O) during hydrothermal. As a result, the carbon content (Carbon content, %C) is greater. In the other hand, hydration is the removal of oxygen in the form of water without causing chemical changes during hydrothermal [27].

2.3.1.3 Decarboxylation

Decarboxylation is a chemical reaction that removes a carboxyl group from a compound and releases carbon dioxide (CO_2) gas. In the other hand, decarboxylation is reaction of carboxylic acid to removing a carbon atom from the carbon chain and adding carbon dioxide to the compound [27].

2.3.1.4 Polymerization

Polymerization is the reaction to combine of small unstable molecules to form larger molecule which more stable [27].

2.3.1.5 Condensation

Condensation is a chemical reaction to combine two molecules forming a larger molecule. Generally, water is a by-product which produces from bioreaction [27].

2.3.1.6 Aromatization

Aromatization is the replacement of hydrocarbon compounds from straight-chain to branched-chain or aromatic compounds using heat and catalyst [27].

2.4 Carbonization process

Carbonization is a pyrolysis process performed by burning raw materials at temperatures below $1,000\text{ }^\circ\text{C}$. Black charcoal, liquid char, tar, and gas are formed depending on the type of raw materials. A porous structure is initiated through the carbonization. During the reaction, non-carbon elements including volatile substances such as hydrogen, oxygen, nitrogen, and water are removed from the structure of the raw material in the form of gas and tar as a byproduct, and the

desired product is char. Char has properties close to carbon with an irregular arrangement of crystalline structures that have a gap (Pore) between the crystals (Porosity) [28].

As a result of the carbonization reaction, other non-carbon atoms such as oxygen, nitrogen and hydrogens are removed as gases. The rest of the carbon atoms are layered. Each layer consists of a hexagonal ring (Aromatic rings) connected in a disordered manner, and form gaps or holes which find the tar and other substances obtained from the burning. After that, the gaps becomes porous with absorbent properties through the stimulation process which leaching tar and other incineration products from cavities or pores. As a result, the adsorption efficiency of the product is due to its chemical structure that caused by the free electrons in unstable state which unsaturated valence, so it needs to bind to other molecules or atoms such as oxygen in the air or other atoms in the substrate. The activation process allows the binding of carbon atoms to form a strong chemical bond often occurs with carbon atoms at the edges of hexagonal circles, allowing them to chemically absorb oxygen at 400-500 °C and convert to oxides surface at higher temperatures ,and also forms strong chemical bonds with hydrogen atoms [29].

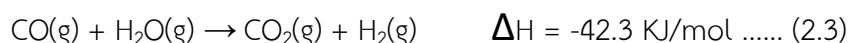
2.5 Pore activation

Activation is the process of converting raw materials into activated carbon in limited oxygen conditions, which is the process of enhancing the adsorption efficiency of activated carbon. In general, there are two methods of stimulation as physical stimulation and chemical stimulation [30].

2.5.1 Physical activation

It is the process to develop and increase pores by oxidizing gas such as carbon dioxide (CO₂) or water vapor (H₂O), etc. using a relatively high temperature in the range of 800-1,100 °C depends on the type of materials. Gasification of oxidizing gas and volatile residues in charcoal and carbon atoms, resulting in a porosity

development in steam activation. The steam used in a superheated steam form to cause organic matter to decompose. When the steam contact with charcoal, a gasification reaction occurs between the water vapor and carbon atoms. The equation is shown as follows.



As a result of this reaction, a gas product (Syngas) is made up of organic substances such as carbon monoxide (CO) and hydrogen (H₂). Equation (2.2) causes the formation of carbon dioxide gas in the system. The equation of stimulation with carbon dioxide gas is shown as follows.



From this reaction, the product gas is carbon monoxide. When most of this fuel gas is released, it will cause a change in the internal structure of charcoal with spongy characteristics scattered. However, the porosity obtained by this method is smaller than that of chemical activation, which affects the adsorption capacity of the activated carbon. This activated carbon is an endothermic reaction. It can be used immediately without having to wash off residual chemicals [31].

2.5.2 Chemical activation

Chemical activation is the production of activated carbon by mixing chemicals that act as stimulants with raw materials. Usually, raw materials have been processed follow by carbonization at different temperatures in the range of about 400-900 °C. Most commonly used chemicals having dehydrating properties such as calcium chloride (CaCl₂), zinc chloride (ZnCl₂), potassium hydroxide (KOH), potassium sulfide (K₂S), potassium thiocyanate (KSCN), phosphoric acid (H₃PO₄), and sulfuric acid (H₂SO₄), etc. and heating with the raw materials to achieve porosity. This chemical plays a role in destroying the original structure of the raw material. When it is

processed through carbonization, some organic elements are decomposed on the surface of the raw material, resulting in a crosslinked structure to form a porous network. In this type of activation, there are still some elements that cannot be degraded resulted in more charcoal and less tar, and the presence of chemicals used in the structure of activated carbon causes less shrinkage. When rinsing off the chemicals, the high porosity of activated carbon is achieved. In this type of activation, there may have problems with the chemical residue in the activated carbon so needs the treatment and purification process before use [32].

2.6 Biodiesel

Biodiesel is a liquid fuel produced from animal fats, vegetable oils, or microalgae including used waste cooking oil through the process of transesterification. Biodiesel has been synthesized through the transesterification by adding alcohol such as methanol or ethanol to fats feedstock with using catalyst such as sodium hydroxide under high temperature conditions to convert fat into fatty acid methyl ester or fatty acid ethyl ester (Fatty acid ethyl ester) depending on the type of alcohol used in the manufacturing process. Glycerol is a byproduct in biodiesel synthesis and can be used in the pharmaceutical and cosmetic industries. Biodiesel usually use as blend with diesel as a fuel in a diesel engine where the mixing rate can be mixed from a percentage of 5%, 10% and 20% due to fuel properties of biodiesel. For example, biodiesel that contains 20% biodiesel mixed with 80% by volume diesel is called B20 so, the number is a ratio of biodiesel in a blending. Biodiesel produced from vegetable oil, animal fats, is a clean and safe fuel for the environment. It can burn completely and the exhaust lower emissions of NO_x (Nitrogen oxides) than diesel when using in diesel engines [33].

2.6.1 Synthesis of biodiesel

The biodiesel production process typically uses 100 parts of vegetable oil reacts with 10 parts of alcohol with a catalyst present to achieve 100 parts biodiesel and 10 parts glycerin through the transesterification process. Transesterification

process commonly used sodium hydroxide or potassium hydroxide as a catalyst while the esterification process usually uses sulfuric or phosphoric acid as a catalyst by mixing the catalyst with alcohol before reacting with vegetable oil. The overall reaction mechanism of biodiesel production or methyl ester formation is shown below.

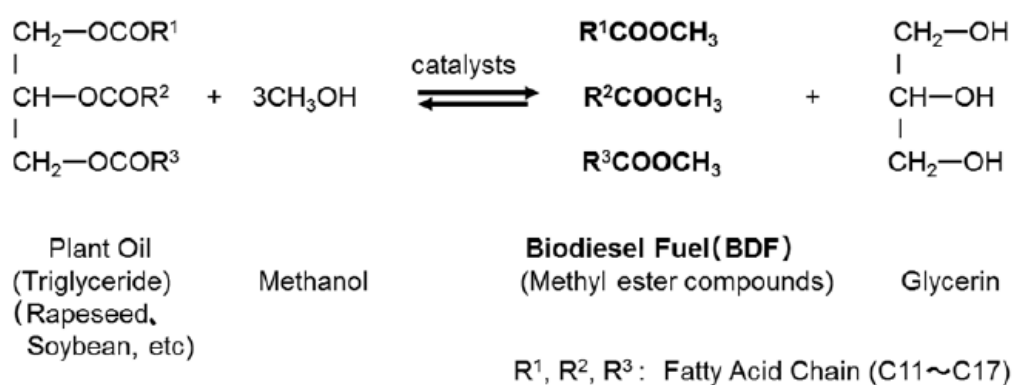


Figure 2.5 Overall reaction of methyl ester formation in transesterification [34].

Biodiesel is a product that has been chemically processed from vegetable oils similar to diesel. However, diesel and biodiesel have different compositions and structures. Biodiesel still has properties that are different from diesel. Some of which are advantages, and some are disadvantages when using biodiesel as fuel compared with diesel. For example, biodiesel has a higher flash point than diesel making it safer to transport, etc [33].

2.6.2 Biodiesel properties

2.6.2.1 Melting point and boiling point

Biodiesel produced from vegetable oil contains many types of methyl ester. According to the number of fatty acids that are constituents of that vegetable oil, the melting point and boiling point of biodiesel depend on the content of methyl ester in the composition. A pure substance has different temperatures that a liquid becomes a solid called melting point or solidification point (Melting point or freezing point). In addition, there are also differences in boiling points. Methyl ester contains

saturated fatty acids and when the structure size of the molecular chain is longer, the melting point will be shifting to a higher temperature, respectively. The boiling point of methyl ester depends on the size of the hydrocarbon chain, independent of the saturated fatty acid content [35].

2.6.2.2 Cold flow properties

Cold flow properties are the ability to operate fuel at low temperatures or in cold climates. For biodiesel with a high freezing point, it does not exhibit good flow properties at low temperatures as diesel. This property was measured using the cloud point and pour point as indicators. The cloud point is the temperature at which the fuel began the wax when the fuel was cooled down, and the pour point was the temperature at which the fuel becomes fully wax (solid) that cannot pump up. In general, the pour point is lower than the cloud point. So, quality biodiesel to be completely liquid [35].

2.6.2.3 Iodine number and oxidation stability

The iodine value of vegetable oil is an indication of the number of double bonds present in that vegetable oil structure. High iodine value vegetable oil means vegetable oils contain a high content of unsaturated fatty acids. When it is used to produce biodiesel, unsaturated fatty acids present in biodiesel will result in accumulation in the tank, fuel transmission system, and filter. High iodine number affects the lower oxidation stability, so biodiesel produced from vegetable oil with high iodine number has a short stored life [35].

2.6.2.4 Heat value

Heat value is indicator of amount of internal energy stored in fuel. In general, both vegetable oil and biodiesel have a lower calorific value than diesel, with a value between 80-85% of diesel [35].

2.6.2.5 Viscosity

The viscosity of biodiesel produced from vegetable oils will have a higher viscosity than diesel at the same temperature. The increasing rate of the viscosity of biodiesel faster than diesel [35].

2.6.2.6 Lubrication

The lubricating fuel property reduces engine wear, especially in diesel engines using biodiesel as a lubricant. Currently, the sulfur content of diesel has been reduced to reduce air pollution. As a result, diesel oil has reduced lubricating properties as the sulfur content is a factor. So, biodiesel has higher lubricating fuel properties than diesel because of higher sulfur content [35].

2.7 Hydrogenation of unsaturated FAME

The full hydrogenation of FAME results in the removal of oxygen and the appearance of new hydrocarbons. Hydrogenation can be produced with or without a catalyst depending on the desired properties of the product. It is difficult to control the selectivity of the hydrogenation reaction without a catalyst so the use of a catalyst can control the selectivity of the desired product. The catalyst will adsorb with the H₂ molecules and promote the reaction. Several researchers report that group VIII metals such as Ni, Co, Pd, Pt, and Rh are catalysts that are often used for partial hydrogenation of C=C double bonds in FAME. Homogeneous catalysts have better activity and cis-C18:1 isomer selectivity in the hydrogenation reaction. Heterogeneous catalysts used in hydrogenation can be promoted the molecules of hydrogen and double bond of FAME to adsorb on the catalyst surface. Hydrogen molecules are divided into 2 hydrogen atoms, then one hydrogen atom is added to the fatty acid double bond in a reversible step. After that, a second hydrogen atom is added to the fatty acid double bond, resulting in hydrogenation an irreversible reaction. The advantage of the heterogeneous catalyst used is that the catalyst easy to separate from the product, so they convenient in the regeneration of the catalyst. where solid catalysts are more popular compared to beef catalysts to increase

catalyst life cycle. Moreover, solid catalysts can work under high-temperature reactions due to their resistance to extreme conditions. Different catalysts were selected for metals with high melting point changes such as Sc, V, Mn, Fe, Ti, Co, Ni, Cr, Cu, and Zn. Many researchers study hydrogenation reactions using noble metals such as Pd, Ru, Rh, and Pt [8] [36].

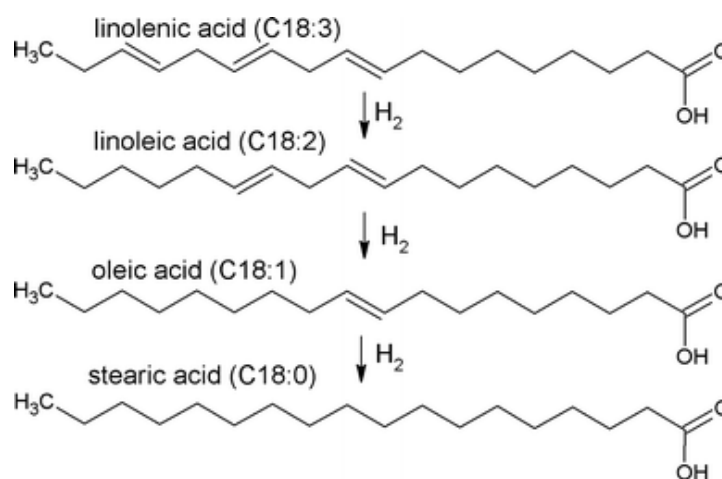


Figure 2.6 Hydrogenation of polyunsaturated FAME [37].

2.8 Catalyst for hydrogenation

A catalyst is a substance that is added to the reaction to accelerates the rate of reaction, allowing the reaction to reach equilibrium faster and no chemical the thermodynamic equilibrium change. This is related to the activated energy and catalyst used to affect to decrease in the activation energy resulting in decrease temperature and pressure required to operate the reaction. Catalyst is separated into two types by the phase of catalyst as homogeneous and heterogeneous catalyst [38].

2.8.1 Homogeneous catalyst

Homogeneous catalyst is a catalyst with the same phase as the Reactant and product such as acid catalyst and base catalyst ie sulfuric acid, sodium hydroxide.

Homogeneous catalysts have better catalytic activity and specificity than heterogeneous catalysts. By the conditions used in the reaction that is mind

conditions and easier to study the mechanism of the reaction because there are no problems with the diffusion of reactants to the catalyst (same phase). The production cost is low and the product decay is minimized because homogeneous catalyst usually uses in ambient conditions, such as atmospheric pressure and temperature, and because of easy to synthesized so the catalyst is inexpensive.

The disadvantage is that it is difficult to separate the catalyst from the reactants and product because they are in the same phase, so it is difficult to reuse the catalyst. The most common methods are solvent extraction or distillation. This type of catalyst often decomposes or deteriorates in harsh conditions (High heat or pressure) affect the homogeneous catalyst life is shorter than the heterogeneous catalyst. After the separation process, a waste management system must be required [39].

2.8.2 Heterogeneous catalyst

Heterogeneous catalyst is a catalyst that its phase is different from the reactant and the substance (non-homogeneous). The heterogeneous catalyst usually in a solid phase such as metals and zeolites, etc. This type of catalyst uses adsorption and desorption mechanisms where the reagents are adsorbed on the surface and react on the catalyst active site. The resulting product is evacuated from the catalyst active site and another reactants molecule absorbs on the surface and continues the reaction cycle. So, a good catalyst must have a good ability to absorb the reactants but absorb less produce. The heterogeneous catalyst is easier to separate from the product and the reactant than the homogeneous catalyst and can be used under high temperature and pressure conditions. Catalysts have a long service life and can be easily recycled but have a disadvantage in the high reaction conditions required and problems with the diffusion of the reactants to the catalyst due to the phases in reaction. Partial hydrogenation generally uses heterogeneous catalyst type in metallic form (M^0). Metallic catalysts is loaded on support material to avoid the problem in agglomeration of metallic catalyst [36, 38, 40].

2.8.2.1 Catalyst (Active species)

Active species is a substance that acts to accelerate the reaction. The catalyst may only contain catalysts, but in cases where the catalyst is expensive or has a low surface area, it is preferable to use the method of catalyst loading on the support. Metallic form is a catalyst generally use in partial hydrogenation reaction due to its activity. In industrial, monometallic catalysts are usually used such as Pd and Pt due to its efficiency but also have a high cost. So, transition metal catalyst such as Mo, Ni, Co, Fe, and Mg has been an alternative for partial hydrogenation reaction due to its lower cost compared with the noble metal but also has low catalytic activity. So, instead of use alone alternative metal, it has been synthesized with noble metal in the bimetallic form to enhance the catalytic activity from the synergistic effect of metals and add other properties such as impurity Torrance effect to the catalyst [39, 41].

2.8.2.2 Support materials

Often use inexpensive substances with a high surface area. The main purpose of the support material is to avoid the agglomeration of catalyst to increase the surface area of the catalyst. In addition, there will be increase interactions between the receptors to increase catalytic activity in some cases. Generally, support materials should be inert within the reaction. Supports can be in the form of granules or powders, the most used in the industry are Al_2O_3 (Alumina), SiO_2 (Silica), and carbon. The key properties of the support are its high surface area and pore volume because it pointing to enhances absorbance and metal dispersion and interaction [39, 41].

2.9 Preparation of catalysts on support

Typically, the metal catalysts can be load on support surface in four methods as precipitation, adsorption, ion exchange and impregnation method. Each method has its pros and cons which must be considered from use.

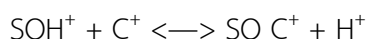
2.9.1 Co-precipitation method

Co-precipitation is the reaction between the powder particles of the carrier and the salts of the solution as oxalates, nitrates, sulfates, and chlorides in a base medium such as NaOH, KOH, NH₄OH, NaCO₃, and NaHCO₃, resulting in a hydroxide or carbonates form of metals are insoluble in water. These substances can be converted to oxides by heating. The preparation was done by mixing the support with the desired amount of salt solution. But in some cases, the support may need to extract air in the support to ensure the absence of air in the pores. After that, the base solution is added to make the precipitate. The next step is filtration or separation and then rinsing out substances, i.e. bases solution which is the ion of the substrate, and the substances on the surface. Co-precipitation is suitable for containing 10-20% of metal content to the activated carbon. if a lower dosage is required, alternative methods should be considered [42].

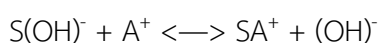
2.9.2 Adsorption

Adsorption is a method to soak supporting material in a salt solution with a suitable concentration for adsorption. Adsorption is a suitable method when a low content of activated elements is required. The disadvantage of the adsorption technique is that the saturation content is low. For example, in nickel and alumina solutions, only 2-3% of the metal content can be prepared it takes a lot of time for higher metal loading. So maybe more appropriate to use other methods. In general, the adsorption mechanism occurs as follows [43].

Equilibrium for the cation (C⁺), where S is the function group.

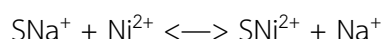


Equilibrium for the anion (A⁻), where S is the function group.



2.9.3 Ion exchange

Ion exchange similar to ionic adsorption in previous method, the difference is that ion-exchange occurs besides protons. Low charged ions such as Na^+ are exchanged with higher charged ions such as Ni^{2+} and the equilibrium occurs as follows (S is any function group).



Ion exchange takes place when the newly replaced ion can bind stronger to support material than the original ion. Mostly when it comes to ion exchange, it looks like soaking support materials in a solution of the metal salt and wait for the exchange ion amount achieved. The advantage of the exchange is limited as it takes a long time and when the exchange is saturated, the ions cannot be increased any further [44].

2.9.4 Impregnation

The impregnation method is the easiest and most convenient method of preparing a catalyst on a support. The supports are immersed in a metal salt solution to saturate the porous support under specified conditions (Concentration, Mixing, Temperature, Time). It also depends on the adsorption conditions on the substrate surface that affect the dispersibility of the catalyst. Especially expensive catalysts, such as noble metals, will not react with the catalyst support. The most widely used supports are alumina, activated carbon, and silica gel. But there are limitations in the preparation of metal loading using the wet impregnation method is the solubility of the substrate metal with water or other solvents. Besides, the support must have Hydrophilic properties and if the support is not wet, the system must be operated under a vacuum or changing the type of solvent to a wetting agent with the carrier used. Typically, the catalytic metal added to the support must be in the range of 10-40% of the support. finally, the impregnated catalyst must be dried and calcined to remove contaminants in the catalyst and also increase the mechanical properties of the catalyst [45].

2.10 Catalyst deactivation in partial hydrogenation of biodiesel

The deactivation of the catalyst in hydrogenation oils is often caused by toxic sulfur and other components present in the oil. Even if all poisoning are eliminated, catalyst deactivation may be caused by side reactions during hydrogenation leading to an intermediates or products such as carbon monoxide or deposition of carbonaceous (coke) which may reduce the catalytic activity. Coke is most likely to occur on catalysts during hydrogenation reactions, but the coke formation that causes catalyst deactivation has not been reported in edible oil hydrogenation. Coke typically causes activity degradation by coating the active site or blocking in the pore network. Coke can be more or less harmful, and the carbonaceous may be take place in the reaction site. Coke formation is often associated with high temperature gas in phase reactions. However, deactivation was also observed by the formation of coke during processes performed at medium and low temperatures, such as the liquid phase hydrogenation of acetylene [17] [46].

2.11 Pore characteristic of porous materials

2.11.1 Classification of porous materials

Porous materials have different pore sizes depending on the synthesis method for different applications. In the IUPAC definition of porosity, the pore size range is used as a criterion for classification. Which can be divided into 3 sizes as follows [47].

- Microporous material: the pore diameter < 2 nm.
- Mesoporous materials: the pore diameter between 2 - 50 nm.
- Macroporous materials: the pore diameter > 50 nm.

2.11.2 Adsorption isotherm

Adsorption isotherm is a representative to describe the distribution of the adsorbent between liquid and solid cycle. The rate of dispersion can be measured at equilibrium and will depend on the adsorbent concentration or the adsorbent

properties. It can be fully absorbed in every position and will weaken the gravity of the sorbent surface due to the less surface position. But it may still be able to absorb the adsorbent molecules, causing second or third adsorption instead, where the second adsorption may occur before the first layer is full at all positions and in some places. The unit may absorb several layers, stacking higher. The shape of the adsorption isotherm provides information about the process of adsorption and the amount of adsorbent on the surface of the sorbent isothermal surface. There are different types of isotherms depending on the type of sorbent. Adsorbents and their interactions between the molecules and the surface of the adsorbent.

Most studies of the absorption equilibrium begin with temperature classification, so exothermic reactions occur in the adsorption isotherm has been used to determine pore size from the adsorption behavior through the curve. This classification of pores is necessary for the theory that explains the adsorption phenomenon. The BET method can describe surface areas. However, the IUPAC implies that the isotherm type will lead to an explanation of the behavior of the adsorption. The classification of isotherms has been divided into six categories according to the IUPAC standard as shown below [47, 48].

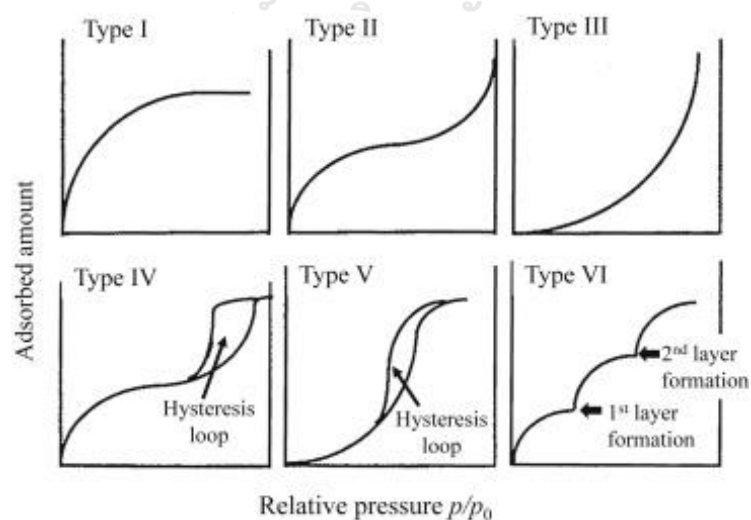


Figure 2.7 IUPAC classification: Physisorption isotherm type [48]

Type I refers to microporous materials. Monolayer adsorption has a chemical adsorption behavior, refer to Langmuir isotherm. The gas adsorption amount increases rapidly under relative pressure (P/P_0). The heat adsorption increases slightly when the relative pressure is close to 1 because the hair follicle is saturated with molecular gas. The material absorbs gas in small pores. (Less than 2 nm pore width) such as activated carbon and zeolite.

Type II refers to the s-shaped isotherm, typically identifying less porosity materials or macroporous materials. The thermal behavioral characteristic is the physical adsorption in which capillary and pore condensation occurs when relative pressure approaches 1. The complete adsorption of the monolayer exhibit knee curve or inflection point at low P/P_0 (0.1 to 0.3). In contrast, the gas molecules are adsorbed on the mono layer, known as the multilayer adsorption process at higher relative pressure.

Type III shows isotherms as the arc of a concave, which is typical of non-porous materials. The adsorption of the monolayer is a weak attraction force.

Type IV refers to a mesoporous structure (The width of pore from 2 to 50 nm), as the isotherms show the hysteresis loop involved in the condensation of pore capillary. The curvature of vapor pressure causes the isotherm adsorption and adsorption at the hysteresis loop. The first stage of the absorption isotherm at low relative pressure is similar to type II, while the adsorption increases rapidly at high relative pressure.

Type V is similar to Type IV isotherms and is similar to Type III due to the interesting force of the relatively weak mono-layer adsorption.

Type VI is a stepped isotherm by layer-to-layer adsorption. Isotherm curve depends on the relative pressure and adsorption temperature. Typically, gases are adsorbed at temperatures close to their melting point [48].

2.12 Literature review

Industrial and transportation is an essential part of the economics in the world so, a large amount of fuel such as gasoline and diesel fuel requirement is increasing every day. Therefore, the depletion of unsustainable fuel source that is a fossil fuel must be a concern nowadays. In addition, Incomplete combustion of fossil fuels affects to increase in pollutant emissions such as CO_2 , CO, SO_2 , PM, and HC that cause an effect on the environment. Therefore, biodiesel is another way of replacing petroleum-based fuels to solve the problem. Biodiesel is a conventional fuel that is less toxic and more lubrication to diesel engines compared to diesel. Biodiesel composed of high amount of polyunsaturated FAME, which easily oxidized. Oxidized polyunsaturated FAME form into slurry-phase that affect to clogged of injector or fuel filter. Other compositions in biodiesel such as water and acid lead to increase corrosion in engine. To solve the problem, many researchers have studied partial hydrogenation of biodiesel to convert polyunsaturated FAME to monounsaturated FAME, which improves oxidation stability. In the other hand, increasing monounsaturated FAME slightly effect decreased of cold flow properties. However, partial hydrogenation operated with mild condition provides low conversion of polyunsaturated FAME. Therefore, a catalyst is required for increased activity and selectivity on cis-isomer in product composition. Noble metals such as Pd and Pt have been reported in excellent catalytic activity. Support materials such as Al_2O_3 , zeolites, SiO_2 , MCM-41, and activated carbon (AC) also used to increase metal dispersion that leads to an increase in catalytic activity. The overview of current studies about this point is summarized in all ideas.

X. Jin et al. [49] This study investigated the effects of chemical type and stimulating ratios in the preparation of lignin-based activated carbon with K_2CO_3 and KOH (40% concentration) in a solution for 16 h. Then, carbonization was performed at 500-900 °C for 20-50 minutes. The chemically activated carbon was studied using the BET and Iodine number technique. K_2CO_3 -activated K_2CO_3 at 800 °C for 50 min was

more effective at absorbing methyl blue and iodine than KOH-activated carbon at the same condition because CO is eliminated when temperature over 600 °C resulting in increased surface area and porosity.

Abdel-Ghani et al. [50] Activated carbon from olive cake waste was synthesized at temperatures of 400 °C. Activation using KOH a ratio of KOH:char at 2:1 and 4:1, then carbonization 600 and 900 °C for 1 and 3 h. The samples were analyzed by BET, FT-IR spectroscopy, and SEM. The result indicated that the olive cake-based AC synthesis through carbonization at 400 °C and then porosity activated using KOH as a stimulant at a temperature of 600 °C for 1 h with a KOH:char ratio of 2:1 exhibit the micro and mesopores with the highest pore area volume at 672 m²/g.

Azadeh B.N et al. [51] studied the different type of base (NaOH and KOH) in pore activation. Base activation was operated at 600-1,000 °C for 1.5 h with base to carbon ratio at 1:1, 2:1 and 3:1. Table 2.10 indicated the higher surface area of carbon founded in high operated temperature and decreased at 1000 C because the collapse of the pores. The ratio of base to carbon at 1:1 insufficient to generated the high porosity of carbon. NaOH generated higher porosity at 2,600 m²/g compared to KOH that generated porosity at 1,600 m²/g. The result indicated that NaOH was suitable to activated porosity of carbon than KOH.

Table 2.3 Effect of activation condition and physical properties of activated carbon [51]

Activation temperature	NaOH:C impregnation ratio	Activation time (h)	SSA (m ² · g ⁻¹)	Activation yield (%)	Pore volume (cm ³ · g ⁻¹)	Micropore volume (cm ³ · g ⁻¹)	Mesopore volume (cm ³ · g ⁻¹)
800 °C	2:1	1	2100	52	1.19	0.64	0.55
800 °C	2:1	1.5	2600	50	1.33	0.62	0.69
800 °C	3:1	2	2300	46	1.12	0.56	0.55
800 °C	2:1	2	2300	49	1.17	0.55	0.62
800 °C	1:1	2	500	76	0.63	0.42	0.21
600 °C	2:1	2	2100	48	1.54	0.75	0.79
1000 °C	2:1	2	600	54	0.50	0.11	0.39

Artita N. R. et al. [52] Studies on whether Pd/MCM-41-silatrane have been shown higher catalytic activity (TOF) than Pd/MCM-41-SiO₂ for partial hydrogenation

of soybean biodiesel at 100 °C and 0.4 MPa of H₂ for 4 h due to dispersion and distribution of Pd particles on MCM-41-SiO₂ better than Pd/MCM-41-silatrane. The Pd/MCM-41-SiO₂ catalyst revealed a more stable dispersion of small Pd particles with support for MCM-41-SiO₂. Moreover, Table 2.7 shows Pd particle size of 12.7 nm, arranged on the outer surface and partially moved into the pore. It can be identified with Pd particles, which appear sufficiently large internal pores of the SiO₂ support, giving C18:0 (more complete degree of hydrogenation) and C18:1 trans isomer. The MCM-41-SiO₂ catalyst provide higher oxidation stability, but the cloud point was found to be lower than Pd/MCM-41-silatrane.

Table 2.4 FAME compositions, TOFs, and ratio of trans/cis C18:1 of Pd/MCM-41-SiO₂ and Pd/MCM-41-silatrane [52]

	Feed	At C18:2 conversion 40%		At C18:2 conversion 60%	
		Pd/MCM-41-SiO ₂	Pd/MCM-41-silatrane	Pd/MCM-41-SiO ₂	Pd/MCM-41-silatrane
FAME composition					
C18:2 (wt.%)	50.95	30.54	29.95	20.69	20.00
C18:3 (wt.%)	5.43	1.18	0.97	0.30	0.29
C18:1 (wt.%)	29.16	45.54	45.79	57.44	55.21
– Trans	–	7.19	7.77	11.55	11.27
– Cis	25.16	38.19	37.99	45.67	44.05
C18:0 (wt.%)	3.68	4.74	4.41	5.48	4.62
TOF ($\times 10^4 \text{ h}^{-1}$)	–	2.42	2.48	2.38	2.52
Degree of complete Hydrogenation (%)	–	2.33	1.59	3.13	1.70
Ratio of trans/cis C18:1	–	0.19	0.20	0.25	0.26

Natthida N. et. Al [53] reported that 2 wt% of Pd loaded on activated carbon support catalyst exhibit good partial hydrogenation activity. The continuous reaction from C18:3 to C18:2, C18:1, and C18:0 was shown in Figure 2.5. Partial hydrogenation of C18:2 and C18:3 to C18:1 show that the selectivity of both reactors is similar at low conversion (78%), while at high conversion, batch reactor resulting in higher selectivity of C18:1 than continuous flow reactor. Although C18:1 selectivity and conversion were high in batch reactor, continuous flow reactors provided conversion rates 4-5 times higher than batch reactor. It can be explained that the oil contact to the catalyst surface in a continuous flow reactor is lower than batch reactor. However, continuous flow reactors are more useful because they have lower operating times compared to batch reactors.

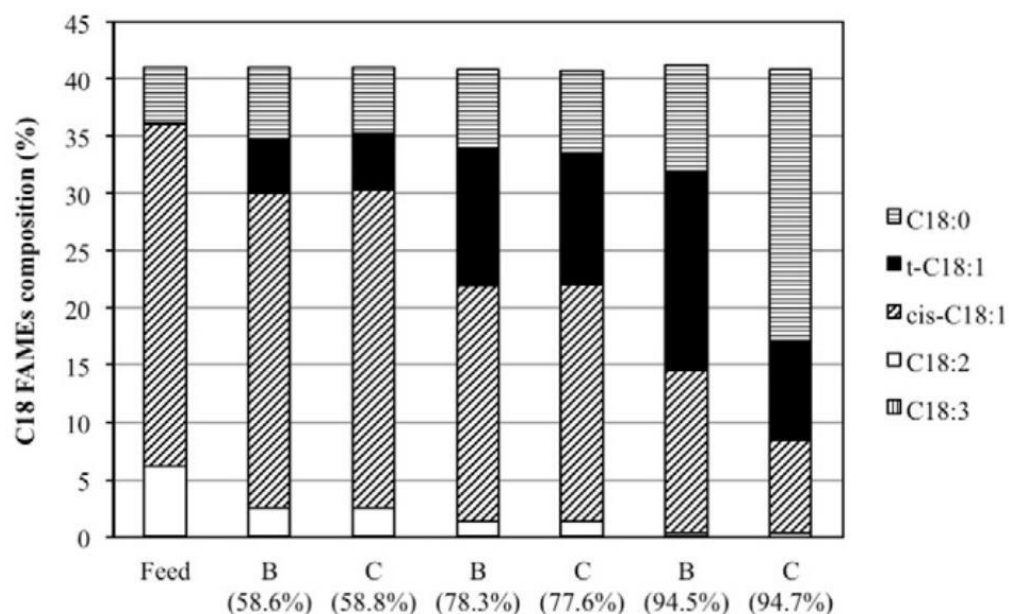


Figure 2.8 Composition of biodiesel feed and H-FAME derived from batch (B) and continuous-flow (C) reactors at different conversions of C18:2 and C18:3 [53]

Natthida N. et al. [54]. Pd/Al₂O₃ was prepared by wet impregnation method and calcination at 500 °C for 3 h and reduced at 100 °C for 2 h for study the partial hydrogenation of BDF rapeseed in batch reactors under 80 °C, 0.3 MPa reaction conditions and flow rate of H₂ at 200 ml/min. Stronger acidic site of Pd/Al₂O₃ provided higher sulfur tolerance than Pd/SiO₂-Al₂O₃. Acidity of supports provides higher sulfur tolerance due to the strong adsorption between Al₂O₃ and the substrate blocking the entrance of sulfur to the Pd active site. In addition, support acidic site leading to increase the selective of cis unsaturated FAME. The oxidation stability was improved from 1.89 h to 33.48 h after 1 h hydrogenation reaction. In other hand, H-FAME exhibited worst cold flow properties that cloud point increased from -3 to 15 °C and pour point from -11 to 12 °C.

Use of noble metal such as Pd catalyst exhibited the excellence in activity through the partial hydrogenation reaction of biodiesel but also having sensitivity to Sulfur and other impurities in biodiesel feedstock. Sulfur content in biodiesel feedstock easier adsorption on metal active site compared with biodiesel feedstock

that direct causing to the decreased in catalytic activity. Many researchers have investigated the effect of transition metal addition such as (Ni, Co, Cu, Mo, and Mg) to prevent the deactivation of catalyst and can be reduced the cost of catalyst in partial hydrogenation reaction.

Jakkaphong J. et al. [55] prepared Ni/SiO₂ catalyst with 10 wt% of Ni loading by incipient wetness impregnation to use as a catalyst for partial hydrogenation of waste cooking oil at 100 °C for 4 h. Ni catalyst has increased the selectivity of monounsaturated FAME. TOF maximum (TOF = 486 h⁻¹) revealed at 1 h of reaction due to a large number of Ni vacancies and after 4 h TOF decreased to 203 h⁻¹ due to the deactivation of catalyst causes a slight decrease in performance. In addition, the Ni/SiO₂ catalyst used in partial hydrogenation increase the biodiesel yield from 97.56% to 98.09% of waste cooking oil.

Chachchaya T. et al [56] studied the effect of Pd, Pt and Ni catalyst in ratio of 1wt%, 1.82wt% and 10% respectively on SiO₂ support. Partial hydrogenation was operated in batch type reactor at 120 °C and 4 bar. Pd/SiO₂ catalyst exhibit the highest TOF in partial hydrogenation that greater than Pt/SiO₂ and Ni/SiO₂ catalysts. In contrast, Pt/SiO₂ catalyst exhibit the most tolerance in sulfur. Three type of metal catalyst used in partial hydrogenation leading to increase of oxidation stability compared with biodiesel feedstock.

Guantao w. et al. [57] investigated the catalytic transfer hydrogenation (CTH) that is the alternative process for partial hydrogenation of jatropha oil biodiesel using Raney-Ni as catalyst via used microwave as a heating source. Catalytic transfer hydrogenation was operated at 85 °C, stirring rate 400 rpm and 100 g of water amount. Raney-Ni catalyst indicated that prevention of poisoning by sulfur atom in jatropha oil feedstock and excellence effective in cis-C18:1 selectivity. CTH method also exhibit a good effective to avoid the generation of cis-C18:0.

Used of Ni in partial hydrogenation exhibit the highest increased in tolerance of sulfur from biodiesel feedstock compared with noble metal such as Pd, and Pt and other transition metals such as Co, Cu and Mo and also have an effective in cis isomer selectivity of C18:1. In addition, Ni catalysts can be reduced catalysts cost in industrial. Some transition metal such as Cu has been reported by A.F. Trasarti et al [51] that also provided the good selectivity in hydrogenated of C18:3 and C18:2 to cis-C18:1 but prevented the formation of C18:0, which provided the good lubricants of biodiesel H-FAME. Natheless, used of transition metals to partial hydrogenation of biodiesel exhibited the low conversion compared with noble metals (Pd and Pt). So, many researchers investigated the synthesized the metal catalysts in bimetallic form to use the prominent of each metals type together.

Chachchaya T. et al. [58] synthesized PdMg/SiO₂, NiMg/SiO₂ and PtMg/SiO₂ catalyst to upgrading soybean biodiesel through partial hydrogenation. Partial hydrogenation was operated at 80–120 °C under 4 bar of H₂ pressure. The result indicated that the PdMg/SiO₂ and PtMg/SiO₂ catalysts exhibited higher conversion of polyunsaturated FAME (C18:2 and C18:3) comparing with catalyst without Mg modified. NiMg/SiO₂ exhibit lower conversion of polyunsaturated FAME because of Ni catalyst active in strong conditions. Mg modified as bimetallic catalysts provided high the selectivity of cis-isomer C18:1 because Mg promoted electron transfer from support material to metal that effect in strong adsorption of metal on support material.

Shane M. et al. [59] investigated the sunflower oil hydrogenation using PtNi/SiO₂ catalyst. Partial hydrogenation of sunflower oil was operated at 200 °C under 3 bar of H₂ pressure for 2-3 h. PtNi/SiO₂ catalyst exhibit the good selectivity of cis-C18:1 and provided 23% of trans-C18:1 compared to Pt/SiO₂ catalyst that provided 26.5%. Ni and Pt metals on SiO₂ formed in individual monometallic and catalytic activity of PtNi/SiO₂ similarly to Pt/SiO₂ catalyst because Ni exhibited the weak interaction between FAME and catalysts.

Yue Z. et al. [60] synthesized the Cu-Ag/SBA15, Cu-Pd/SBA15 and Ni-Ag/SBA15 catalysts for partial hydrogenation of soybean biodiesel. The results indicated that the Cu-Ag/SBA15 provided 1.8 times higher C18:2 selectivity comparing with Cu-Pd/SBA15. Ni-Ag/SBA15 provided 1.3 times higher C18:2 selectivity comparing with Cu-Pd/SBA15. The precious metal can be improved the primary catalyst distribution leading to improved catalytic activity and reduced trans-C18:1 formation in partial hydrogenation. Ni-Ag/SBA15 provided 50.27% of C18:3 and TFA content decreased to 10.43%



CHAPTER 3

RESEARCH METHODOLOGY

In this study the experimental works were divided in 2 steps (Fig. 3.1). First, synthesis of nanoporous carbon (NPC) from cattail leaves (CL) including with preparation and characterization of bimetallic PdNi on NPC support was examined. Finally, catalytic testing in partial hydrogenation of palm biodiesel was also conducted for confirming the possible performance and deactivation of the resultant PdNi catalyst impregnated on NPC. The details of all experimental methodologies and characterization techniques will be described in this chapter.

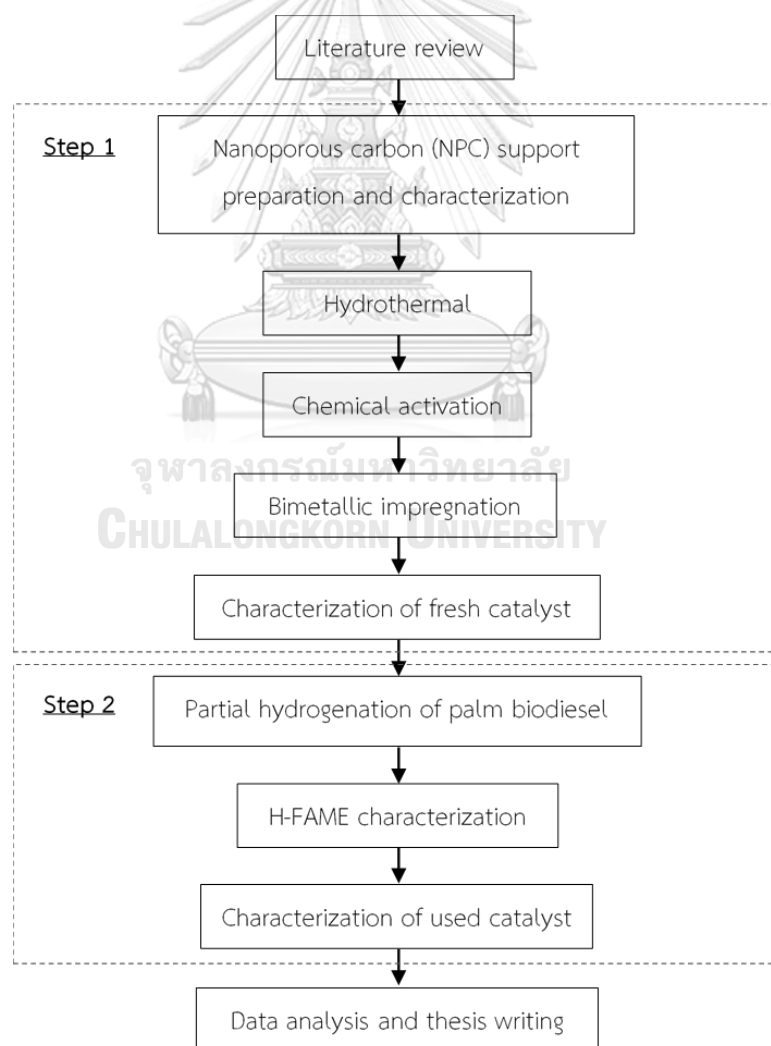


Figure 3.1 Schematic diagram of research methodology

3.1 Nanoporous carbon preparation

Cattail leaves (CL) derived from King Mongkut Institute of Technology Ladkrabang (KMITL) has been used as carbon source to prepare nanoporous carbon (NPC). CLs were dried at 110 °C then cut and meshed into the powder. The CL powder were sieved to achieve a particle size of 2 μm. To produce hydrochar (HC), 30 g of CL was mixed with 60 ml of DI water then packed into the autoclave to hydrothermal at 200 °C for 12 h. After the hydrothermal reaction, the autoclave was quickly cooled to room temperature to stop the reaction immediately. Hydrochar (HC) was dried at 90 °C for 12 h to ensure that the water was eliminated. Chemical activation was used to promote the porosity of nanoporous carbon. 10 g of HC were stirred in 4 M concentration of KOH solution at 80 °C for 2 h. The mixture of HC was filtered using Buchner funnel with the vacuum pump, then dried to evaporate water in solution. After that, dried HC were placed in the horizontal tube furnace to carbonization at 900 °C for 2 h with 100 ml/min of nitrogen flow rate and heating rate 10 °C/min. Finally, nanoporous carbon (NPC) was washed with 0.5 M of HCL and distilled water until achieving pH of 7.

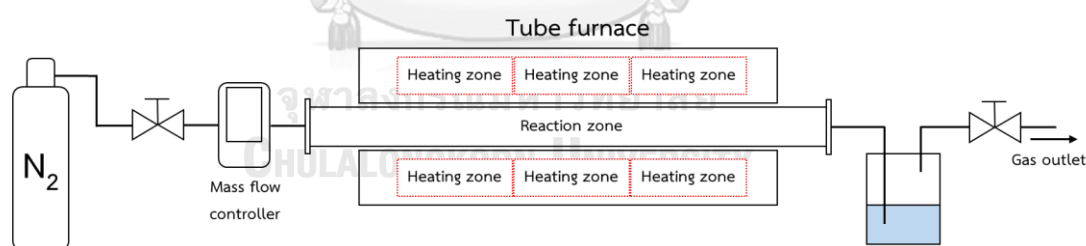


Figure 3.2 Schematic diagram of Horizontal tube furnace for chemical activation of cattail leave to produce nanoporous

3.2 Characterization of nanoporous carbon

Nanoporous carbon from cattail leave synthesized through hydrothermal carbonization process (HTC) as described above was used as a catalyst support. Characteristics of NPC has been investigated by proximate and ultimate analysis, scanning electron microscope (SEM), Fourier transform infrared spectroscopy (FTIR)

and Nitrogen sorption. The specifications of the characterization techniques are explained as follows.

3.2.1 Proximate and ultimate analysis

Proximate analysis is often used for thermogravimetric characterization elements of nanoporous carbon and biomass, where the weight loss can be explained by thermal degradation of the sample under inert gas or oxygen gas. Carbon composition consists of moisture, ash and volatiles, and fixed carbon content. Traditionally, moisture represents the mass of water in a dry sample, which is defined by the ASTM E-871 method (ASTM, 2014). Volatile matters are converted to organic compounds such as CO, H₂ and CH₄ with ASTM E-872 and ASTM E-1755 method. Ash refers to inorganic compounds that are left after the sample is completely oxidized. The ash content was analyzed by D-1102 or UNE-EN 14775. The fixed carbon content was determined by the difference using equation to this equation: %FC = 100-%VM%M-%A. Dried sample 0.1 g was heated in 2 stages. First, the temperature was heated from 30 to 800 °C with a slope rate of 10 °C/min under nitrogen atmosphere for pyrolysis and for removal of volatile matter and moisture. Finally, the inert gas is replaced by air atmosphere and the sample were oxidized after 800-1000 °C in combustion.

The ultimate analysis estimates the composition of nanoporous carbon, solids, and gases in term of the proportions of chemical elements. The carbon content (C), hydrogen (H), oxygen (O), nitrogen (N) was determined using the CHN element analyzer (CHNS628 series). The carbon content including with combustion gas released from organic matter. The hydrogen content is also related to coal, which exists in the form of moisture and water. All different elements can be calculated with oxygen percentage via the following formula as $O = 100 - (C + H + N)$. The NPS 5 mg was rapidly sintered from 30-950 °C with a heating rate of 10 °C/min under He and O₂ atmosphere.

3.2.2 Surface functional and morphology analysis

Scanning electron microscope (SEM) was used to analyze the morphology of catalyst and support by zeiss EVO MA10. The samples were taped on a carbon tape and put onto specimen stubs. Then, samples were coated with gold (Au) by sputtering technique under vacuum atmosphere to enhance electrical conductivity on the samples surface. The coated samples were scanned in secondary electron mode and operated at 10 kV. The magnification used at 500x, 1000x to receive high resolution images.

Fourier transforms infrared (FTIR) spectroscopy was used to investigate the surface functional group to specify the organic and inorganic molecule by the vibration of bond while adsorbing wavelength in infrared range. A surface functional group were analyzed by PerkinElmer UATR Two using ATR transmission mode. The samples were packed and pressed onto ATR crystal material. IR scan were use in range of 400 to 4,000 cm^{-1} with 8 cycles of scan rate.

3.3 Catalyst preparation

Nanoporous carbon was used as a support material for catalysts. Tetraamminepalladium (II) chloride monohydrate $[\text{Pd}(\text{NH}_3)_4\cdot\text{Cl}_2\cdot\text{H}_2\text{O}]$ and Nickel (II) nitrate hexahydrate $[\text{Ni}(\text{NO}_3)_2\cdot 6\text{H}_2\text{O}]$ for 98% purity were used as metal precursors. Catalysts were synthesized by wet impregnation technique. Monometallic catalysts (Pd/NPC and Ni/NPC) were prepared by using 1 wt% for Pd and 5 wt% for Ni catalyst due to its catalytic activity. Bimetallic catalyst (PdNi/NPC) was prepared by using mixture of Pd and Ni contained 1% and 5% of metal catalyst respectively. Metal precursor solutions were mixed with 10 g of nanoporous carbon at temperature of 60 °C and dried by using rotary evaporator with vacuum atmosphere until completely evaporated. After that, catalysts were calcined at 500 °C for 3 h under nitrogen atmosphere with 10 °C/min for heating rate.

3.4 Catalyst characterization

The characteristics of prepared catalysts have been investigated by different techniques, such as X-ray diffraction (XRD), scanning electron microscope (SEM), energy dispersive spectrometry (EDS), N₂ adsorption/desorption and temperature programmed reduction (TPR), CO chemisorption. The specifications of characterization techniques are explained as follows.

3.4.1 X-ray diffraction (XRD)

X-ray diffraction technique was used to investigate crystallinity to identify crystal structure, crystallite size, and confirmed metal formed on surface of prepared catalysts. X-ray diffractograms were obtained by Rigagu Smartlab X-ray diffractometer with Guidance software. The source of x-ray is Cu-K α radiation ($\lambda=1.5418 \text{ \AA}$) with an accelerating voltage of 40 kV and the current of 40 mA. X-ray sources and detectors scanned from 10 to 90° with theta-2-theta mode in steps of 0.02°/s. The Debye-Scherrer equation can determine the crystallite size of catalyst.

3.4.2 Transmission electron microscopy (TEM)

The transmission electron microscopy analysis identified the internal morphology and loaded metal catalyst particles on catalyst support. TEM micrographs were obtained by JEOL TEM-2100Plus with an accelerating voltage of 200 kV. The sample was sonicated to be suspended in ethanol and then dropped onto carbon-coated copper grids. The distribution of metal particle size was analyzed by ImageJ (National Institutes of Health (NIH), Bethesda, MD, USA) software.

3.4.3 Energy dispersion spectrometry (EDS)

Energy dispersion spectrometry identified the elemental distribution on surface, and quantitative analysis of catalyst. The elemental analysis of catalyst can be determined by X-ray fluorescence analysis. Results were shown in atomic ratio and color mapping.

3.4.4 CO chemisorption

Metal dispersion on the catalyst was performed by using Ohkura Riken R6015-S, expressed as the ratio of the total number of metal atoms on the metal surface. Metal dispersion was calculated by assuming that the atomic ratio of CO to the metal surface is 1:1. The U-quartz tube reactor contained 0.03 g of quartz wool and 0.1 g of catalyst. The samples were reduced at the same temperature as H₂-TPR at a flow rate of 25 mL/min using a heating rate of 10 °C/min and operated for 3 hours, then cooled to 25 °C in a nitrogen flow. The CO injected 20 µL until absorption saturation was obtained at 30 °C. The CO output gas was detected by a thermal conductivity detector (TCD) observed by a mass spectrometer. The amount of CO adsorption was calculated by the difference between the CO amount detected at the outlet and the amount of CO injected at the inlet. The cubic particle model was used to calculate the catalyst particle size and metal distribution on catalyst.

3.5 Partial hydrogenation of palm biodiesel

The catalysts were reduced at 300 °C (Pd) and 400 °C (Ni and PdNi) for 2 h. Partial hydrogenation of biodiesel was operated in a 300 ml batch type reactor. First, palm biodiesel 200 ml and 1.75 g of catalyst were added to the autoclave. The system was flushed with nitrogen to purge air in the reactor. To find the optimal condition which prevent catalyst deactivation, hydrogen was fed to the reactor with varied hydrogen pressure constant in reactor at 3-5 bar and operating temperature at 60-140 °C. Then, the stirring rate was varied at 250-500 rpm to study the mechanical damage to catalysts. The samples were collected every 30 min, total reaction time was 4 h.

3.6 Biodiesel analysis

Compositions in some pre-hydrogenation and post-hydrogenation biodiesel were collected and inspected using the GC-2010 gas chromatograph equipped with a flame ionization detector and a capillary column (HP-88, 100 m x 0.25 mm x 0.2

μm). Helium was used as a carrier gas with a flow rate of 53.8 mL/min. A sample of 1 μl was injected into an oven at 170 °C after 40 min. The nozzle is increased to 230 °C with a rate of 4 °C/min. The detector temperature was fixed at 250 °C with a 50 for split ratio and maintained for 2.5 min, with 65 min total analysis time. FAME compositions were identified by compared with reference. The ratio of the area under the peak was calculated to define the FAME compositions.

The oxidation stability of the biodiesel was analyzed by Rancimat 743. The flask containing a 7.5 g sample was heated to 110 °C with 10 L/h for airflows. The air was passed through the sample and then fed into a collection vessel containing a 60 mL DI and conductivity probe. Oxidation stability of the samples was shown in terms of the induction period (IP). The IP explained the difference time between the start of the test and conductivity that increase immediately in the collective flask. Typically, the IP value is expressed for time and long IP times of biodiesel fuel, indicating high stability against oxidation.

The cold flow properties of the biodiesel were indicated in terms of cloud point and pour point, which were examined by using the Tanaka MPC-102 Tech pour/cloud tester developed in accordance with ASTM D6749. Biodiesel 70 ml was added to the tester glass flask. The biodiesel sample was cooled to less than 0 °C and then heat up until reach 45 °C. Before the collected the sample, the sample was cooled down to room temperature.

CHAPTER 4

RESULTS AND DISCUSSION

4.1 Characteristics of cattail leaves-derived nanoporous carbon

Cattail leaves (CLs) were used as feedstocks to synthesize the nanoporous carbon (NPC) via hydrothermal process and KOH activation. The effects of hydrothermal and activation process are provided in this section.

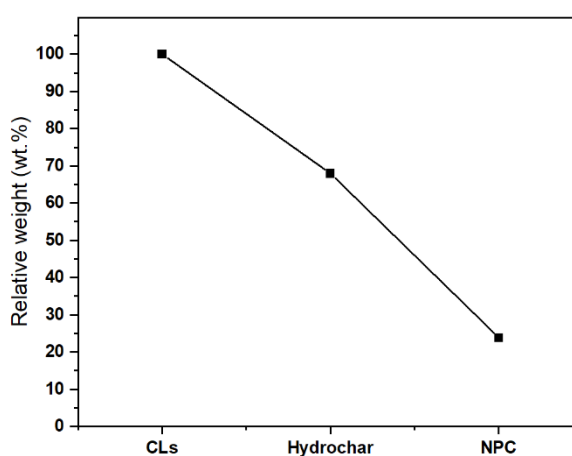


Figure 4.1 Yield of CLs-derived NPC.

Figure 4.1 demonstrates the yield of hydrochar at 200 °C for 24 h and chemical activation using 4 M of KOH as an activating agent at carbonization temperature of 900 °C for 2 h. The CLs hydrochar produced from the decomposition of organic substance in biomaterials structures (composed of cellulose, hemicellulose and lignin) was found to be approximately 67.97 wt% yield. The hydrothermal process relies on heat and pressure to allow water molecules to diffuse into the structure of the cattail leaves and destroy the structure of cellulose and hemicellulose, which causes the long-chain polymer to break into a short polymer. The short polymer chain also decomposes into gases such as hydrogen (H₂), carbon monoxide (CO) and carbon dioxide (CO₂), forming the carbon atom. This is the main factor affecting the reduction of the mass of cattail leaves. After activation process, the NPS yield is gradually decreased to 23.88 wt% because of

concentration of activating agent leading to increase of activation degree [61]. Furthermore, the carbonization temperature influences the decomposition of the hydrochar structure to the tar and gases such as hydrogen (H_2), oxygen (O_2), nitrogen (N_2), and water evaporated from the structure causes cavities within the substance, thus forming porous area.

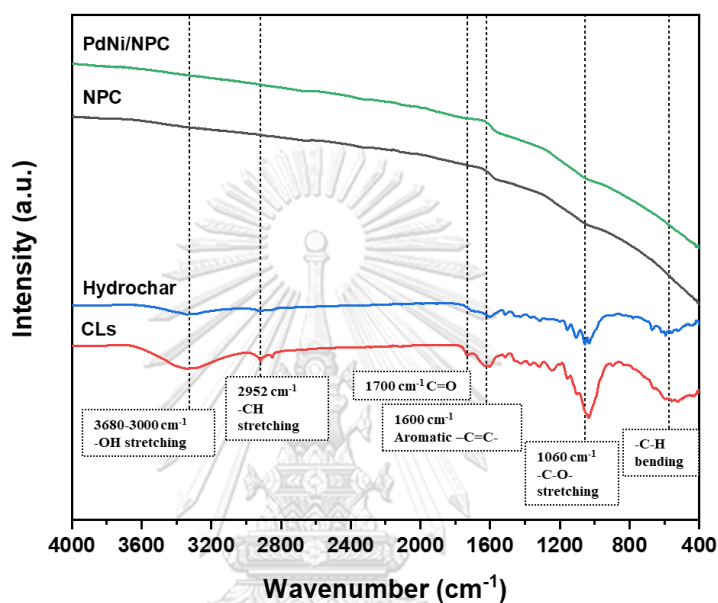


Figure 4.2 Fourier transform infrared spectroscopy (FTIR) spectra of CLs-derived NPC and post-loaded catalyst.

The functional groups on the surface of the cattail leaves (CLs), CLs hydrochar, CLs derived NPC and PdNi/NPC catalysts were exhibited in **Figure 4.2** and **Table 1**. It was indicated that after the hydrothermal treatment process at 200 °C for 12 h, the OH-stretching ($3680-3000\text{ cm}^{-1}$) peak was reduced, which is a slight hydroxyl group of lignin due to high thermal stability of its structure. The reduction of the peak CH-stretching (2925 and 2850 cm^{-1}) from aliphatic degradation and a significant decrease of CO stretching from ether group of cellulose and hemicellulose [62], which has low thermal stability. The decomposition of cellulose and hemicellulose during the hydrothermal process could form an aromatic group structure from aromatization, which is shown at 1600 , 1512 , 1460 , and 790 cm^{-1} peaks. Additionally,

a new C=O vibration (1700 cm^{-1}) peak is formed during the hydrothermal process, which is a component of the carboxylic, ketone and aldehyde group formed by dehydration of the hydroxyl groups from the decomposition of cellulose and hemicellulose [63]. After undergoing pore activation and carbonization at $900\text{ }^{\circ}\text{C}$ for 2 h, the structure of cellulose, hemicellulose, and lignin was completely decomposed. Compared to the pre-carbonization period, a large number of aromatic groups occur on the surface due to the decomposition of tar and volatile substances such as hydrogen, oxygen, nitrogen, and water evaporation from the structure within the substance, and become porous [28, 29]. When a metal catalyst is impregnated onto a nanoporous carbon, it was found that there was no change in the functional group characteristics because no functional group forming occurs between the metal catalyst and the support surface.

Table 4.1 Functional groups of the CLs, CLs hydrochar, CLs derived NPC and PdNi/NPC.

Wavenumber (cm^{-1})	Functional group	Description
3680 - 3000	O-H stretching	Hydroxyl or carboxyl groups, alcohols from cellulose or phenols from lignin
3000 - 2800	C-H stretching	Aliphatic
1700	C=O stretching	Carbonyl, ester or carboxyl from cellulose and lignin
1600 and 1512	C=C stretching	Aromatic skeletal present in lignin
1380 - 1240	C-O stretching	Vibration in lignin
1290 - 950	C-O stretching	Hemicellulose esters
1420	C-H bending	C-H deformation in lignin and carbohydrates
1060	C-O stretching	Vibrations in cellulose and hemicellulose
860 - 724	C-H bending	Aromatic

The proximate and ultimate analysis of CLs, CLs hydrochar and CLs derived NPC was shown in **Table 4.2**. It can be separated into moisture, volatile matter, fixed carbon, and ash. The fixed carbon and ash content is the main component in CLs because the carbon atom is the main component of organic substance and ash plays significant role in various utilization [64]. Hydrochar was produced from the cattail leaves through the hydrothermal process where volatile matter in the cattail leaves structure (Cellulose, Hemicellulose, and Lignin) was removed and thus increased its fixed carbon content. After the activation and carbonization respectively, NPC was produced. After complete carbonization, fixed carbon and ash content also increased from evaporation of volatile matter. Fixed carbon observed in proximate analysis is gradually increased from 33.28 to 81.18%. Typically, activated carbons composed with the fixed carbon content over 70% and 2-10% for ash content. Increasing of ash represents the decreasing of porosity, which leads to decreased specific surface area from the matrix of carbon [65, 66].

Table 4.2 Proximate and ultimate analysis of cattail leaves (CLs).

Properties	Proximate analysis (wt.%)				Ultimate analysis (wt.%)			
	M	VM	FC*	A	C	H	N	O*
Raw CLs	1.58	75.90	20.31	2.21	39.95	4.46	1.74	53.85
Hydrochar	1.63	62.31	33.28	2.78	45.45	45.45	45.45	45.45
NPC	1.59	10.41	81.18	6.82	86.35	4.67	1.64	7.34

* Calculated by different, M: moisture, VM: volatile matter, FC: fixed carbon, A: ash, ** (as-received basis, w/w).

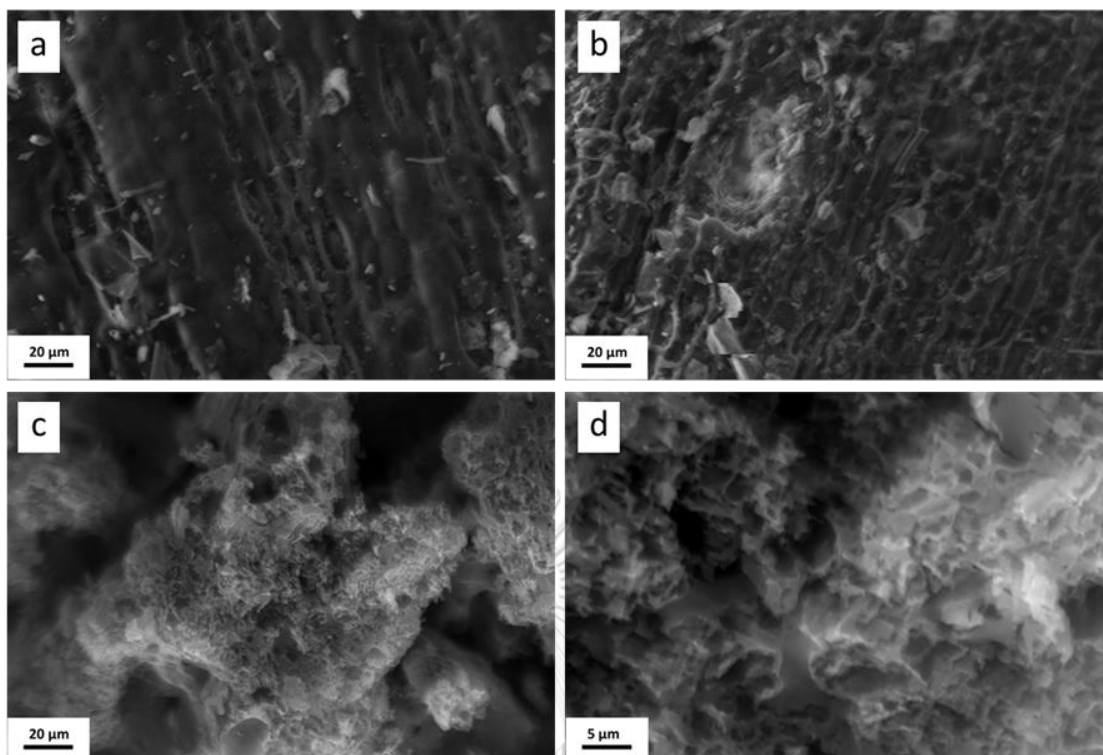


Figure 4.3 Scanning electron microscope (SEM) micrographs of (a) CLs, (b) CLs hydrochar, (c) CLs-derived NPC at 500x and (d) 2000x magnification.

The surface morphology of CLs and NPC were examined by scanning electron microscopy (SEM) technique at magnification of 500x and 2000x as shown in **Figure 4.3**. It was shown that there is no porous structure on CLs. Dense and smooth surface was exhibited on external surface. After hydrothermal carbonization (HTC) process, it was indicated that various pores and cavities were dispersed on the surface of the nanoporous carbon support, which was caused by KOH activation [67]. Due to the high amount of potassium ions, pore expansion and channeling occurs. Its pore size covered in the nanopore size, which mostly found in mesopore and some of micropore at the surface of NPC. The fracture structure occurs due to high temperature of carbonization and KOH activated conditions and physical fracture from external impact during the process.

The dispersion of 6 wt% bimetallic PdNi catalyst at a Pd:Ni ratio of 1:5 on the carbon support was shown in **Figure 4.4**. It was indicated that metallic particles were

well dispersed on the surface of the nanoporous carbon support. For analyzing the elements qualitatively and quantitatively, EDX (Energy Dispersive X-ray) demonstrated the pattern and dispersibility of monometallic metals on the surface in the form of colored dots to confirm that metal catalyst has been impregnated onto the support surface. Wet impregnation method could generate well dispersion pattern of metallic catalysts particles on the surface of NPC. A rotary evaporator has been used to dry catalysts, and pressure reduction was applied to allow air to be sucked out of the porous area on the support surface, allowing the metal particles in solution type flow within the porous area formed on the support surface [68].

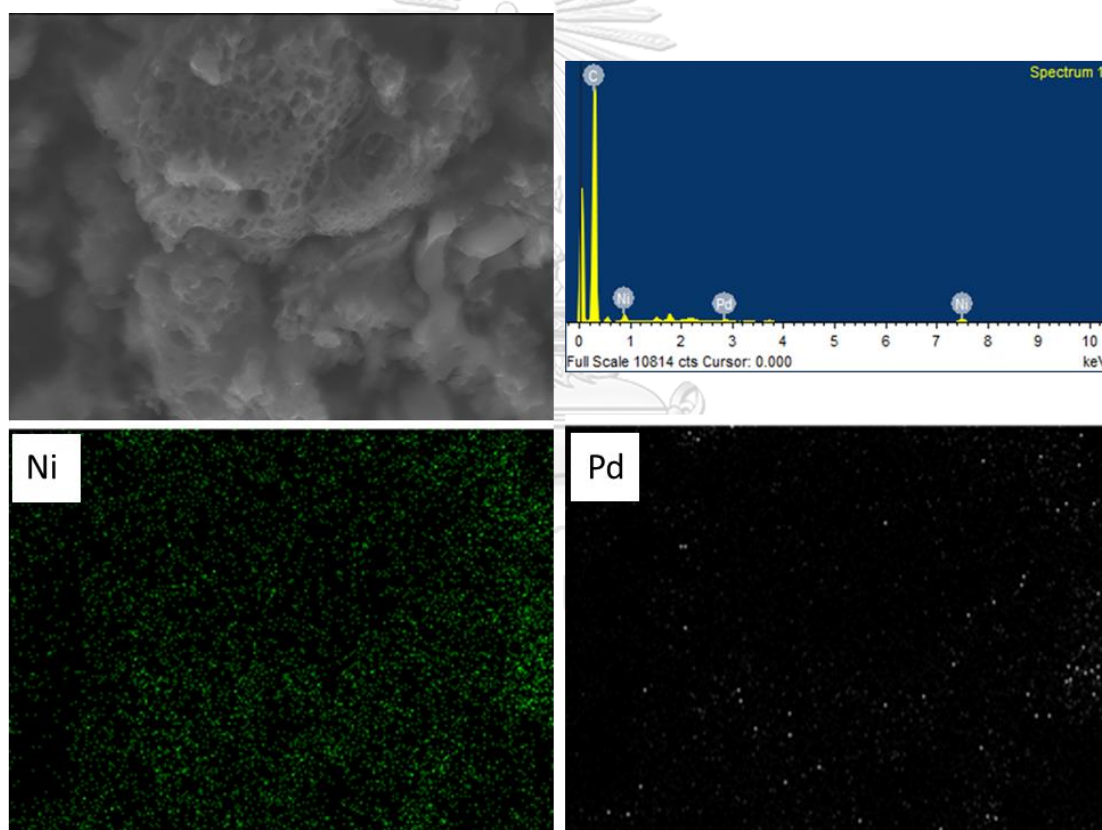


Figure 4.4 Energy dispersed X-ray (EDX) spectra of PdNi/NPC.

The internal morphologies detailed of CLs derived nanoporous carbon support (NPC), monometallic (Pd/NPC and Ni/NPC) and bimetallic (PdNi/NPC) were observed by TEM. **Figure 4.5** represented the TEM micrograph, the results indicated a disordered hierarchical porous structure, which contains innumerable pores [69]. The

gaps between disordered carbon layers suggest that the existence of mesopore and micropore in NPC. In addition, the particle size of metallic Pd and Ni on NPC from TEM images were observed at 6.5 ± 1.6 and 11.3 ± 1.9 respectively.

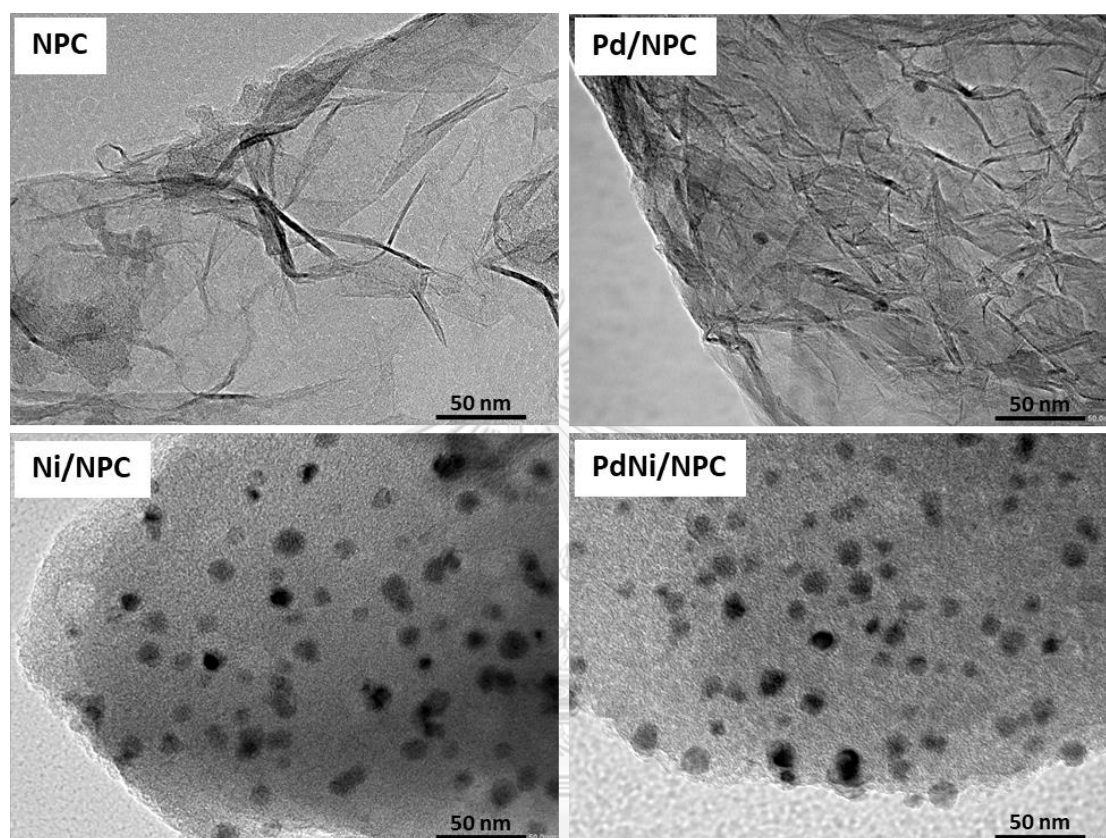


Figure 4.5 TEM micrograph of the NPC, Pd/NPC, Ni/NPC and PdNi/NPC catalysts.

The N_2 adsorption and desorption isotherms of NPC and catalyst PdNi/NPC are shown in **Figure 4.6(a)**. According to the IUPAC classification [70], this isotherm exhibited hysteresis loop type IV, indicating the presence of mesopore (2-50 nm) and some of micropore (>2 nm). KOH activation at 900 °C for 2 h could generate pore size suitable for allowing substance with high viscosity molecule such as biodiesel and gas reactant to react with the active site dispersed on pore surface [71]. **Figure 4.6(b)** shows pore size distribution calculated by DFT method. Most of pores observed were in the range of 1.6-4.4 nm, and small distribution also observed at pore size range of 20-60 nm, which confirmed predominant mesopore and some of micropore presence in the carbon. The S_{BET} of PdNi/NPC was $2187.96 \text{ m}^2\text{g}^{-1}$, which

was higher than NPC ($2002.12 \text{ m}^2\text{g}^{-1}$) caused by the presence of metallic particle on pore surface. Moreover, PdNi/NPC exhibited S_{BET} higher than Ni/NPC ($2139.16 \text{ m}^2\text{g}^{-1}$) and Pd/NPC ($2022.34 \text{ m}^2\text{g}^{-1}$) because of the higher metal loading to nanoporous carbon ratio leading to increasing of catalyst surface area (Table 4.3).

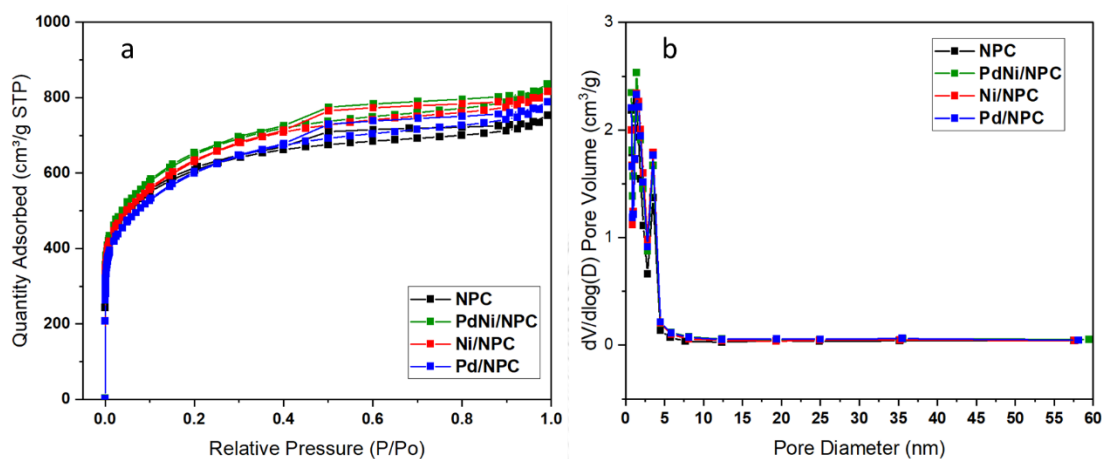


Figure 4.6 (a) N_2 adsorption and desorption isotherms and (b) pore size distribution of NPC, Pd/NPC, Ni/NPC and PdNi/NPC.

Table 4.3 Textural properties of CLs-derived NPC, Pd/NPC, Ni/NPC and PdNi/NPC

Sample	S_{BET} (m^2g^{-1})	D_{av} (nm)	V_{total} (cm^3g^{-1})	$V_{\text{mic.}}$ (cm^3g^{-1})	$V_{\text{mes.}}$ (cm^3g^{-1})
NPC	2002.12	2.63	1.573	0.280	1.239
Pd/NPC	2037.34	2.71	1.601	0.285	1.261
Ni/NPC	2142.16	2.82	1.667	0.296	1.31
PdNi/NPC	2187.96	2.96	1.730	0.308	1.363

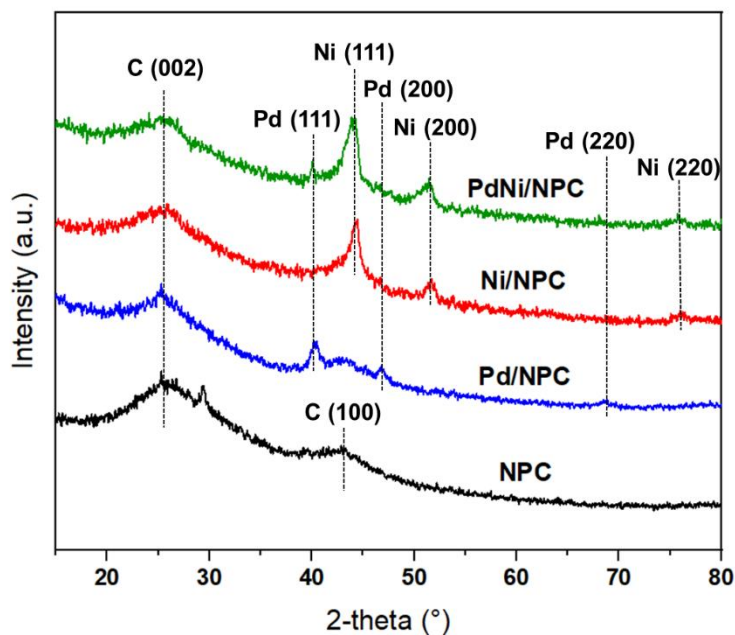


Figure 4.7 XRD patterns of the NPC, Pd/NPC, Ni/NPC and PdNi/NPC catalysts.

XRD patterns of CLs-derived NPC, Pd/NPC, Ni/NPC and PdNi/NPC catalysts were shown in **Figure 4.7**. NPC shows broad peaks at 24° and 43.5° assigned to (002) and (100), which are the planes of carbon materials [72] exhibited in nanoporous carbon support. These broad peaks clearly show the amorphous carbon structure and disordered arrangement of the carbon rings. The Pd metal peaks exhibited at 40, 46.5 and 68.5 were assigned to (111), (200) and (220) planes of metallic form of Pd. The Ni metal peaks exhibited at 44.8, 52.4 and 74.12 assigned to (111), (200) and (220) planes of metallic form of Ni. The diffraction peak of metallic exhibited in monometallic and bimetallic catalysts confirmed that the metal has been loaded on the surface of nanoporous carbon support (NPC).

4.2 Catalytic activity in partial hydrogenation of palm H-FAME

4.2.1 Effect of reaction temperature

Effect of operating temperature of partial hydrogenation of palm BDF at a constant operating pressure of 4 bar for PdNi/NPC catalyst was shown in **Table 4.4** and **Figure 4.8**. Increasing operating temperature of partial hydrogenation reaction improved the conversion of polyunsaturated FAME (C18:2 and C18:3), resulting in poor cold flow properties. At high temperatures (above 120 °C), cis-C18:1 isomer was rapidly converted to trans-C18:1 and later hydrogenated to C18:0 (**Figure 4.9**), higher content of C18:0 results in gradual increase of oxidation stability and cloud point. The high reaction temperature has a significant influence on the isomerization of cis-C18:1 because of the faster reaction rate according to higher molecular kinetic mobility and collision of molecules. In contrast, the formation of trans-C18:1 and C18:0 at 80 °C and 100 °C was lower due to the low isomerization reaction. Therefore, the reaction temperature of 100 °C is optimal to improve palm biodiesel fuel properties as the oxidation stability significantly increased from 13.68 h to 18.12 h. In addition, increase of cis-C18:1 isomer increases cloud point from 12 to 15 °C.

Table 4.4 Effect of temperature on FAME compositions and biodiesel properties of palm BDF and H-FAME over Pd/NPC, Ni/NPC and PdNi/NPC at a reaction time of 4 h.

FAME composition (%)	Palm BDF	H-FAME			
		80	100	120	140
C18:0	3.81	4.4	4.57	4.97	15.82
C18:1	38.65	38.66	40.16	35.49	37.04
cis C18:1	38.57	38.53	39.94	34.51	19.96
trans C18:1	0.08	0.13	0.22	0.98	17.08
C18:2	10.92	9.38	9.26	9.3	0.14
C18:3	0.18	0.14	0.12	0.17	0.05
Conversion of C18:2	-	14.16	15.20	14.84	98.7
Biodiesel properties					
Oxidation stability (h)	13.69	15.21	18.12	17.56	30.12
Cloud point (°C)	12	14	15	15	24

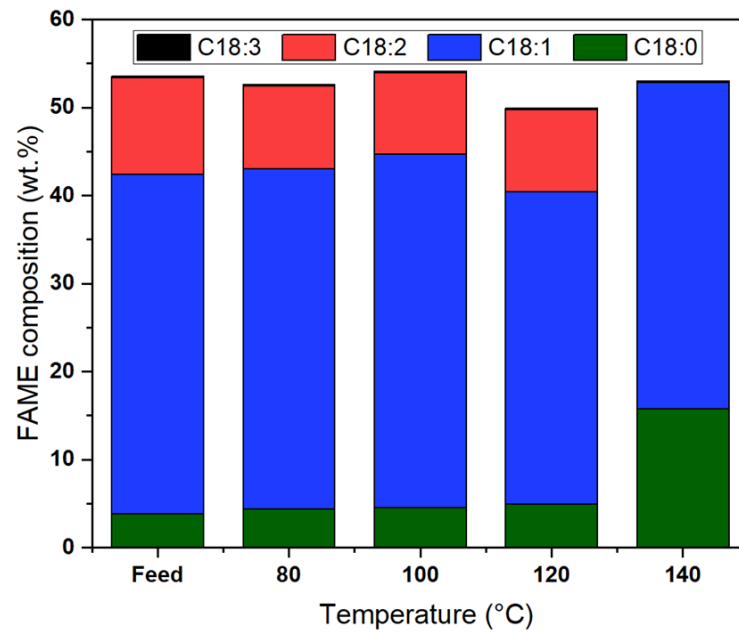


Figure 4.8 Effect of temperature on C18 composition.

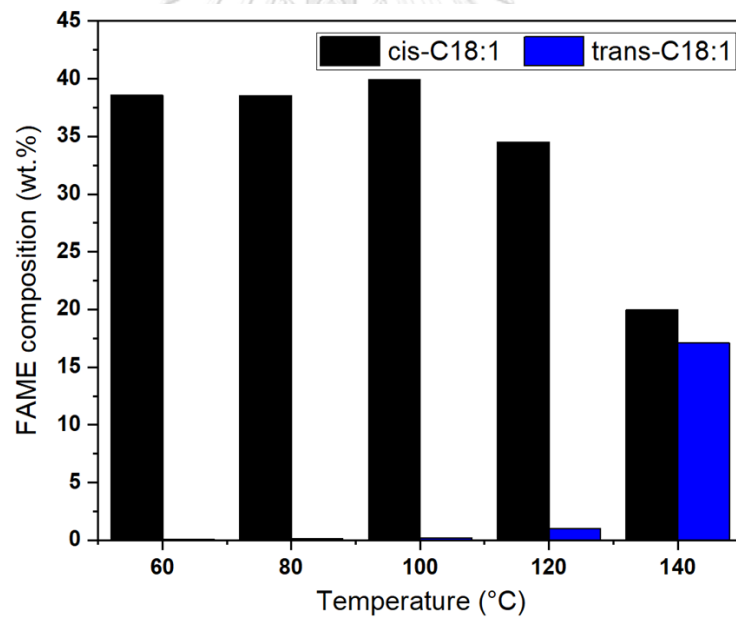


Figure 4.9 Effect of temperature on cis/trans-isomer of C18:1 composition.

4.2.2 Effect of reaction pressure

As the operating temperature at 100 °C was found to be the optimal condition to improve fuel properties of palm biodiesel, the effect of operating pressure on partial hydrogenation of palm BDF was investigated at 100 °C using PdNi/NPC catalyst, and the results are shown in Table 4.5 and **Figure 4.10**. Cis and trans isomers of C18:1 at various temperatures were shown in **Figure 4.11**. While increasing operating pressure, polyunsaturated FAME (C18:2 and C18:3) also converted to C18:1 and later to C18:0. The lower C18:2 and higher C18:0 led to increasing of oxidation stability. At operating pressure of 5 bar, C18:0 composition is only slightly increased from that of 4 bar. Therefore, the reaction pressure of 4 bar was suitable for operation, providing significant increase of oxidation stability from 13.69 to 18.12 h. Note that there was only slight improvement of oxidation stability when operating at 5 bar.

Table 4.5 Effect of pressure on FAME compositions and biodiesel properties of palm BDF and H-FAME over Pd/NPC, Ni/NPC and PdNi/NPC at reaction time of 4 h.

FAME composition (%)	Palm BDF	H-FAME		
		3	4	5
C18:0	3.81	4.45	4.57	4.63
C18:1	38.65	38.91	39.16	39.58
cis C18:1	38.57	38.76	38.94	39.4
trans C18:1	0.08	0.16	0.22	0.18
C18:2	10.92	9.2	9.26	9.28
C18:3	0.18	0.17	0.12	0.14
Conversion of C18:2	-	15.75	15.21	15.02
Biodiesel properties				
Oxidation stability (h.)	13.69	17.8	18.12	18.28
Cloud point (°C)	12	14	15	15

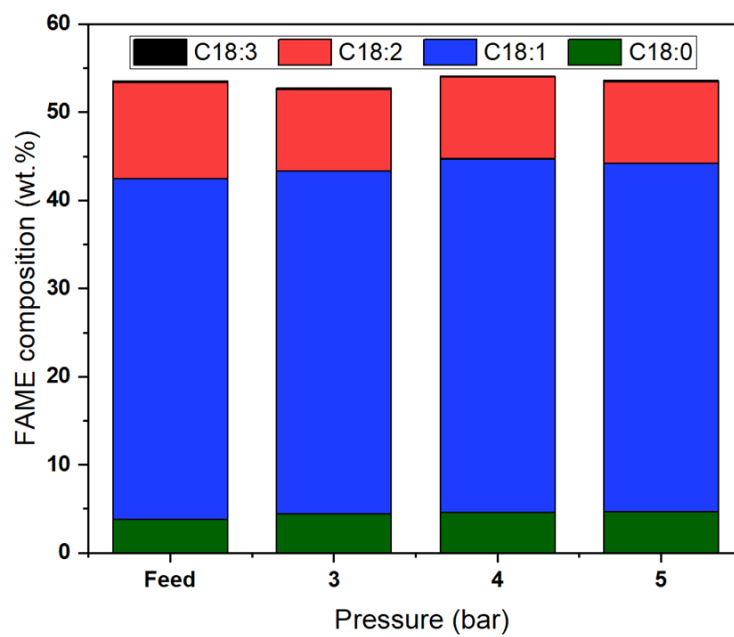


Figure 4.10 Effect of operating pressure on C18 compositions.

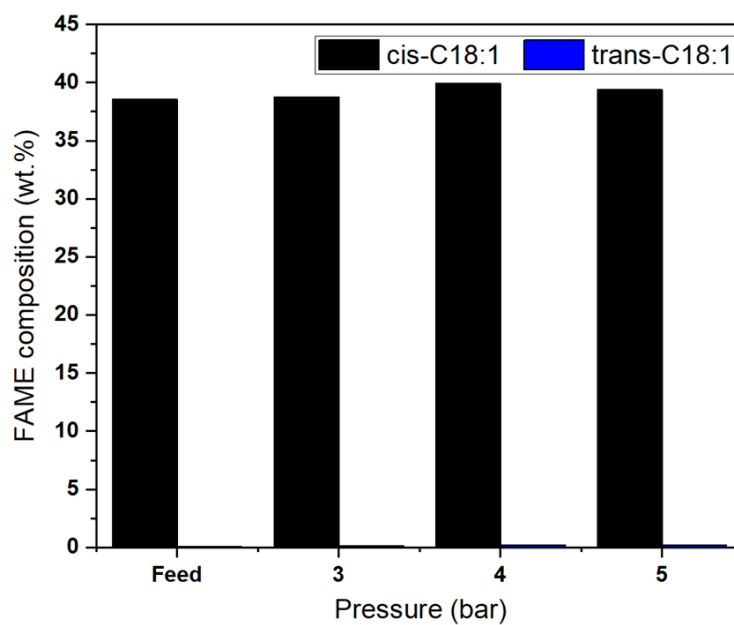


Figure 4.11 Effect of operating pressure on cis/trans-isomer of C18:1 compositions.

4.2.3 Effect of catalyst type (monometallic and bimetallic catalysts)

The FAME composition in the produced palm H-FAME is shown in **Table 4.6** and **Figure 4.12**. The conversions of poly FAME using different catalysts are ordered as follows: PdNi/NPC > Pd/NPC > Ni/NPC, indicating that the monometallic catalytic activity of active metals of Pd is significantly more active than Ni because Ni active is at a high temperature range (>400 °C) [73]. Although Ni shows less catalytic activity, Ni exhibited the very high selectivity of cis isomer of C18:1 than Pd as shown in **Figure 4.13**. Bimetallic of Pd and Ni catalyst was observed the high catalytic activity and cis-C18:1 isomer selectivity, which are the dominant properties of Pd and Ni because of the synergistic effect occurring between metallic particles [74, 75]. Bimetallic PdNi exhibited higher conversion of C18:2 than monometallic Pd and Ni. Metal Ni can adsorb sulfur in palm BDF instead of Pd, which can prevent Pd from sulfur deactivation that would result in reduction of Pd catalytic activity. Correlation of oxidation stability and cloud point was observed. After partial hydrogenation of palm BDF, the oxidation stability was increased from 13.69 to 18.12 h for PdNi/NPC catalyst, 16.33 h for Pd/NPC and 14.10 for Ni/NPC. According to existing biodiesel standards including international standard EN14214 (>8 h), ASTM D6751 (>3 h) and Thai national standard (>10 h), so the produced palm H-FAME can be used to blend with diesel at high ratios such as B10-B30. Cloud point of the produced H-FAME is 14-15 °C, meeting the Thai national standard (>16 °C) [76].

Table 4.6 FAME compositions and biodiesel properties of palm BDF and H-FAME over Pd/NPC, Ni/NPC and PdNi/NPC at reaction time of 4 h.

FAME composition (%)	Palm BDF	H-FAME		
		Pd/NPC	Ni/NPC	PdNi/NPC
C18:0	3.81	4.42	4.20	4.57
C18:1	38.65	39.16	37.75	40.16
cis C18:1	38.57	36.61	37.65	39.94
trans C18:1	0.08	2.76	0.10	0.22
C18:2	10.92	9.29	10.01	9.26
C18:3	0.18	0.14	0.16	0.12
Conversion of C18:2	-	14.93	8.30	15.21
Biodiesel properties				
Oxidation stability (h.)	13.69	16.33	14.1	18.12
Cloud point (°C)	12	14	14	15

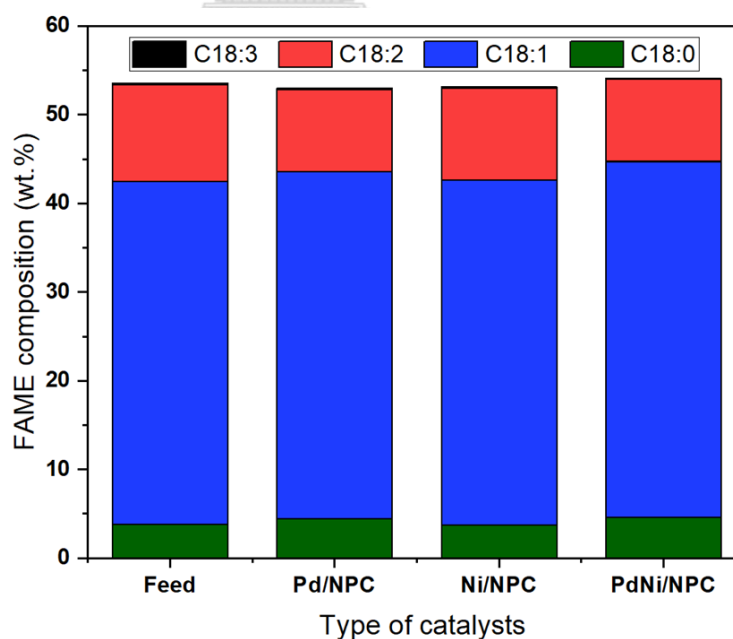


Figure 4.12 Effect of catalyst type (monometallic and bimetallic catalyst) on C18 compositions.

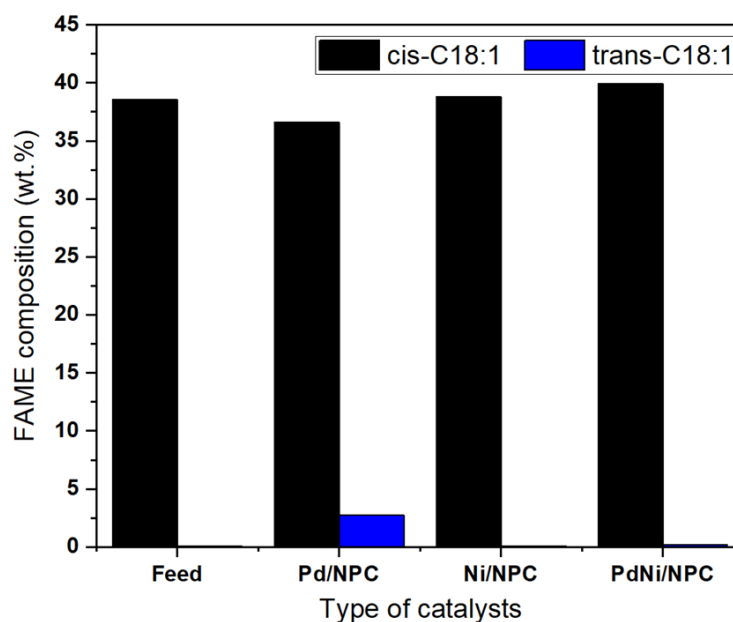


Figure 4.13 Effect of catalyst type on cis/trans-isomer of C18:1 composition.

4.3 Deactivation of catalysts in partial hydrogenation

4.3.1 Effect of reaction temperature

Morphology of PdNi/NPC catalyst after partial hydrogenation reaction at various temperatures: 80 °C, 100 °C, 120 °C and 140 °C were shown in **Figure 4.14**. After operating temperature was raised up, no significant changes in catalyst morphology, BET surface area and metal dispersion of PdNi/NPC catalyst before and after partial hydrogenation at various temperatures were observed as shown in **Table 4.7**. Surface area of the fresh catalyst and used catalyst at 80 °C, 100 °C, 120 °C and 140 °C exhibited S_{BET} at 2139.16 m^2g^{-1} , 2129.43 m^2g^{-1} , 2127.11 m^2g^{-1} , 2118.77 m^2g^{-1} and 2124.46 m^2g^{-1} , which have no significant change with temperature. After partial hydrogenation, dispersion of active metal was gradually decreased from 48.53% to 23.78%, which decreased approximately 50% compared to the fresh catalyst likely due to active metal covered by products originated during the reaction and agglomeration of metal [46]. In addition, no significant difference was observed at different reaction temperatures.

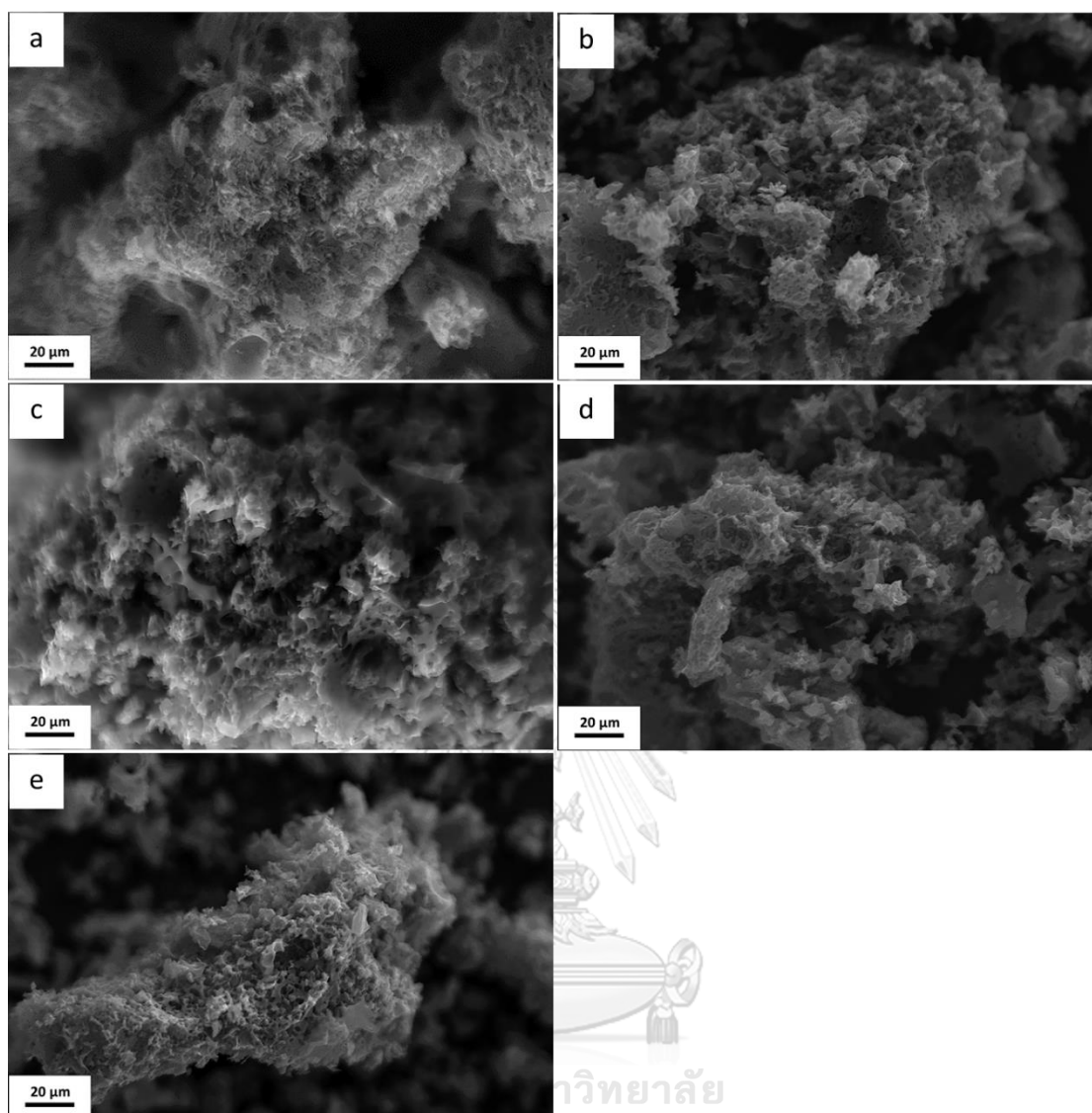


Figure 4.14 SEM images of PdNi/NPC catalyst (a) before and after partial hydrogenation at different temperatures (b) 80 °C, (c) 100 °C, (d) 120 °C and (e) 140 °C.

Table 4.7 BET surface area and metal dispersion at various temperatures.

Temperature (°C)	S_{BET} (m^2g^{-1})	Metal dispersion* (%)
Fresh catalyst	2139.16	48.53
80	2129.43	24.46
100	2127.11	23.94
120	2118.77	25.57
140	2124.46	23.78

*Determined by H_2 chemisorption

4.3.2 Effect of reaction pressure

Morphology of PdNi/NPC catalyst after partial hydrogenation reaction at 100 °C at different pressures: i.e., 3 bar, 4 bar and 5 bar were shown in **Figure 4.15**. By increasing operating pressure, no significant change in catalyst morphology, BET surface area and metal dispersion of PdNi/NPC catalyst before and after partial hydrogenation was observed as shown in **Table 4.8**. Surface area of the fresh catalyst and used catalyst at 3 bar, 4 bar and 5 bar exhibited S_{BET} at 2139.16 m^2g^{-1} , 2131.37 m^2g^{-1} , 2127.11 m^2g^{-1} and 2104.25 m^2g^{-1} . Noted that slight decrease of the value at high pressure could be caused by collapse of pore. After partial hydrogenation, dispersion of active metal was gradually decreased from 48.53% to 23.12%, which was approximately 50% of the fresh catalyst. In addition, there was no significant difference for different reaction pressures.

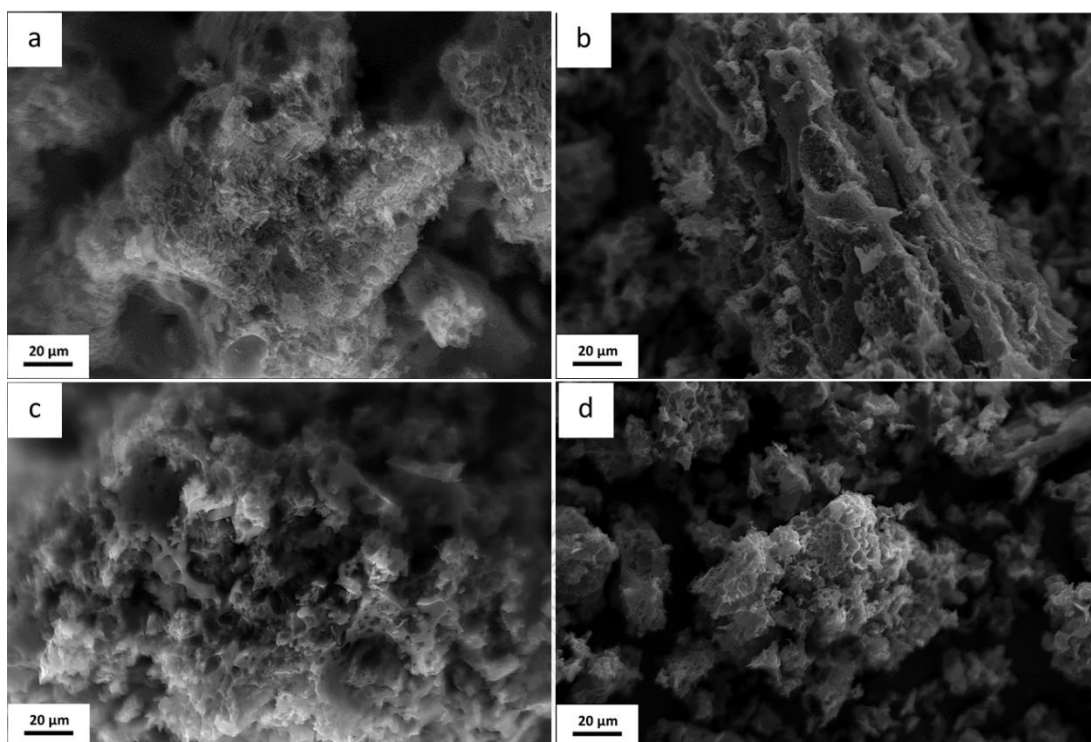


Figure 4.15 SEM images of PdNi/NPC catalyst (a) before partial hydrogenation, and after partial hydrogenation at different pressures (b) 3 bar, (c) 4 bar and (d) 5 bar.

Table 4.8 BET surface area and metal dispersion at various pressure.

Pressure (bar)	S_{BET} (m^2g^{-1})	Metal dispersion* (%)
Fresh catalyst	2139.16	48.53
3	2131.37	24.48
4	2127.11	23.94
5	2104.25	23.12

*Determined by H_2 chemisorption

4.3.3 Effect of stirring rate

Morphology of PdNi/NPC catalyst after partial hydrogenation reaction at various stirring rates: i.e., 150 rpm, 200 rpm and 300 rpm were shown in **Figure 4.16**. The reactions were operated at 100 °C and 4 bar. When increasing stirring rate, fracture of catalyst was observed. BET surface area and metal dispersion of PdNi/NPC catalyst before and after partial hydrogenation at different stirring rates are shown in **Table 4.9**. Surface area of the fresh catalyst and used catalyst at 150 rpm, 200 rpm and 300 rpm exhibited SBET at 2139.16 m²g⁻¹, 2127.11, m²g⁻¹, 2100.12 m²g⁻¹ and 1835.23 m²g⁻¹, respectively. At high stirring rate, catalyst surface area was increased, due to the collision and impact damage occurred between catalyst particles. After partial hydrogenation, dispersion of active metal was decreased from 48.53% to 23.94% at low stirring rate (150 rpm) and slightly increased up to 25.31% at 300 rpm because the fracture of catalyst structure also increased the surface area of catalyst. The used catalyst decreased approximated 50% of metal dispersion compared to the fresh catalyst, because the active metals were covered by products originated during the reaction and agglomeration of metals.

Table 4.9 BET surface area and metal dispersion at varied stir rate.

Stir rate (rpm)	S _{BET} (m ² g ⁻¹)	Metal dispersion* (%)
Fresh catalyst	2139.16	48.53
150	2027.11	23.94
200	2000.12	25.03
300	1835.23	25.31

*Determined by H₂ chemisorption

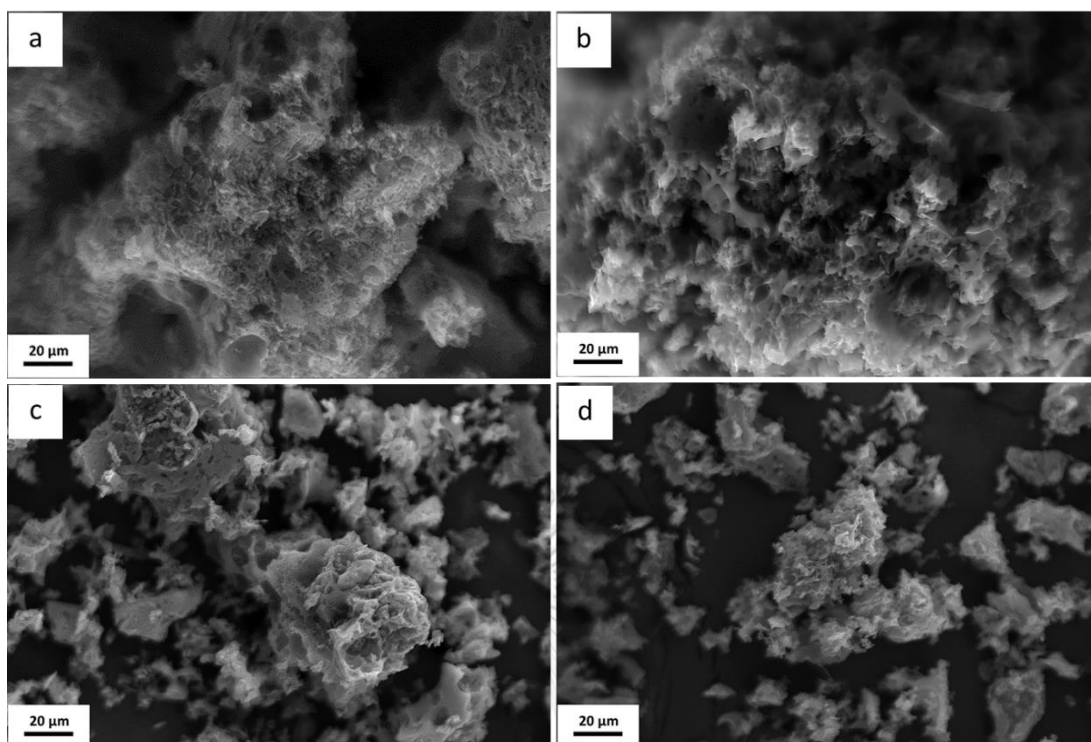


Figure 4.16 SEM images of PdNi/NPC catalyst (a) before partial hydrogenation, and after partial hydrogenation at different stirring rates (b) 250 rpm, (c) 500 rpm and (d) 750 rpm.

4.3.4 Catalyst stability

Catalytic activity profile was shown in **Figure 4.17**. The activity of both Pd/NPC and PdNi/NPC catalysts was gradually decreased at the second batch and lower decreased until remaining the almost stable at the fifth batch. The PdNi/NPC catalyst exhibited higher catalytic activity in several batches compared to the Pd/NPC catalyst. The result suggests that the presence of Ni in bimetallic PdNi catalyst can prevent the deactivation of the Pd catalyst, which caused from the poisoning by sulfur [77] and phospholipids [78] atom in feedstock.

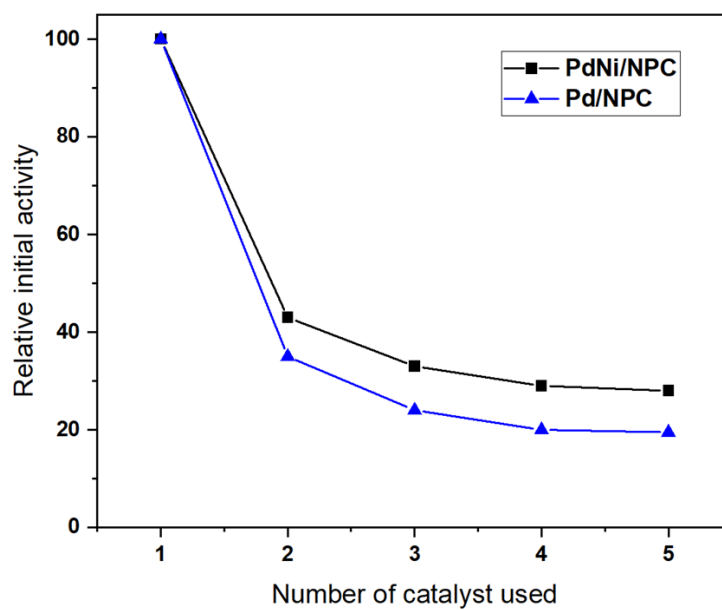
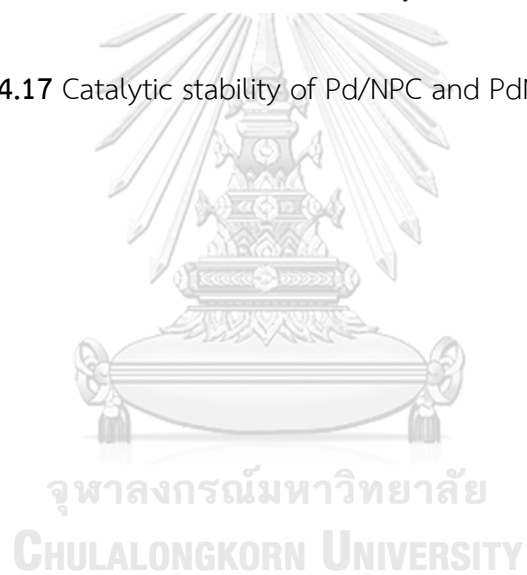


Figure 4.17 Catalytic stability of Pd/Ni/NPC and Pd/NPC catalyst.



CHAPTER 5

CONCLUSIONS

The experimental results described in chapter 4 consist of the synthesis of cattail leaves-derived nanoporous carbon support, catalytic activity in partial hydrogenation of palm H-FAME and catalyst deactivation under various partial hydrogenation conditions. The optimal condition and experimental parameters could be summarized in this chapter.

5.1 Conclusions

5.1.1 Synthesis of cattail leaves-derived nanoporous carbon support

Cattail leaves-derived nanoporous carbon (NPC) was successfully synthesized by hydrothermal carbonization with chemical activation using KOH as an activating agent. The results revealed that the activation by 4 M KOH at 900 °C for 2 h could offer high surface area up to 2139.16 m²g⁻¹. The prepared carbon contained predominant mesopore (2-50 nm) and some of micropore (<2 nm) in carbon matrix. The prepared nanoporous carbon exhibited high carbon content of 86.35% and low ash content (6.82%). Therefore, the prepared nanoporous carbon was used as catalyst support. The monometallic and bimetallic of Pd and Ni were impregnated on the nanoporous carbon and the catalyst was dried by using a rotary evaporation technique. The X-ray diffraction exhibited no alloy phase in PdNi/NPC catalyst. The PdNi/NPC catalyst had 48.53% of metal dispersion determined by H₂ chemisorption technique.

5.1.2 Catalytic activity in partial hydrogenation of palm H-FAME

The palm H-FAME was successfully synthesized with PdNi/NPC catalyst at 100 °C and 4 bar as an optimal condition, which offered the highest oxidation stability at 18.12 h. For monometallic catalyst, Pd/NPC exhibited higher activity than Ni catalyst because the partial hydrogenation was operated in a favorable temperature range of

Pd. In contrast, The Ni/NPC catalyst exhibited the very high selectivity of cis isomer of C18:1. For bimetallic catalyst, the PdNi/NPC catalyst exhibited the higher conversion than the monometallic Pd/NPC, showing highest catalytic activity, because of synergistic effect between metals. Ni atom is more favorable to sulfur atom than Pd atom. Therefore, Ni loading can prevent the Pd from deactivation. According to existing biodiesel standards including international standard EN14214 (>8 h), ASTM D6751 (>3 h) and Thai national standard (>10 h), the produced palm H-FAME can be used to blend with diesel at high ratio such as B10-B30. Cloud point of the produced H-FAME of 15 °C also meets the Thai national standard (>16 °C).

5.1.3 Deactivation of catalyst in partial hydrogenation

Scanning electron microscopy micrograph technique was employed to examine the morphology of catalyst surface at various conditions such as temperature, pressure and stirring rate. The morphology of catalyst remains the same at various temperatures and also show small change on porosity at various pressures, but fractural structure was found at high stirring rate from collision of catalyst particles. For dispersion of active metal on catalyst surface, the used catalyst decreased approximately 50% (from 48.53% to 23.94%) of metal dispersion compared to the fresh catalyst, as a result of coverage of active metal by products originated during the reaction and agglomeration of metal particles.

5.2 Recommendations

5.2.1 The production of carbon support from other biomasses should be studied.

5.2.2 The effect of metal particle size should be analyzed to demonstrate the deactivation from particle size effect.

5.2.3 The long-term catalytic stability and regeneration should be future studied to demonstrate the catalyst lifetime.

5.2.3 The continuous process of partial hydrogenation reaction should be studied, and the process could be further scaled up for potential application in commercial-scale production.





APPENDIX A
RAW MATERIAL DATA

A.1 Specification data of palm biodiesel (B100)

Customer/Supplier: Patum Vegetable Oil Company Limited (PVO)

Table A.1 Specification of palm biodiesel (Fatty Acid Methyl Ester: FAME) B100

Test Parameter	Test Method	Limitation	Result
Methyl Ester, %wt	EN 14103	96.5 Min	98.0
Density at 30 °C, Kg/m ³	ASTM D 1298	860 - 900	864.1
Viscosity at 40 °C	ASTM D 445	3.5 – 5	4.4
Flash point, °C	ASTM D 93	120 Min	>120
Water, mg/kg	EN ISO 12937	500 Max	210
Acid Value, mgKOH/g	ASTM D 664	0.50 Max	0.16
Iodine Value, gI ₂ /100 g	EN 14111	120 Max	50.4
Appearance	Visual	Clear	Clear



APPENDIX B

BASIC CALCULATION

B.1 Poly-FAME (C18:2 and C18:3) conversion

$$\text{Conversion of C18:2 and C18:3} = \frac{(C18:2 + C18:3)_{\text{before}} - (C18:2 + C18:3)_{\text{after}}}{(C18:2 + C18:3)_{\text{before}}}$$

B.2 Calculation of volume of H₂ adsorption on catalyst

$$V_{\text{ads}} = \frac{V_{\text{inj}}}{m} \times \sum_{i=1}^n \left(1 - \frac{A_i}{A_f} \right)$$

where V_{inj} is volume injected, 0.02 cm³

m is mass of catalyst used, g

A_i is area of peak i

A_f is area of last peak

B.3 Calculation of metal active sites

$$\text{Metal active site} = V_f \times \frac{V_{\text{ads}}}{V_g} \times N_A$$

Where S_f is stoichiometry factor, H₂ adsorbed on metal, H:metal = 2:1

V_{ads} is volume adsorbed

V_g is molar volume of gas at STP, 22414 cm³/mole

N_A is Avogadro's number, 6.023×10²³ molecules/mole

B.4 Calculation of metal dispersion

$$\text{Metal dispersion (\%)} = 100 \times \frac{\text{weight of metal from H}_2 \text{ adsorbed}}{\text{weight of metal loaded}}$$

$$\%D = 100 \times S_f \times \frac{V_{\text{ads}}}{V_g} \times \frac{MW}{\%M} \times 10000$$

Where S_f is stoichiometry factor, H₂ adsorbed on metal, H:metal ratio = 2:1

V_{ads} is volume adsorbed

V_{g} is molar volume of gas at STP, 22414 cm³/mole

MW is molecular weight of the metal



REFERENCES

1. Nelson WL. Petroleum refinery engineering: McGraw-Hill; 2018.
2. Murugesan A, Umarani C, Subramanian R, Nedunchezian N. Bio-diesel as an alternative fuel for diesel engines—a review. *Renewable and sustainable energy reviews*. 2009;13(3):653-62.
3. Knothe G. Biodiesel and renewable diesel: a comparison. *Progress in energy and combustion science*. 2010;36(3):364-73.
4. Huang D, Zhou H, Lin L. Biodiesel: an alternative to conventional fuel. *Energy Procedia*. 2012;16:1874-85.
5. Nabi MN, Akhter MS, Shahadat MMZ. Improvement of engine emissions with conventional diesel fuel and diesel–biodiesel blends. *Bioresource Technology*. 2006;97(3):372-8.
6. Vedaraman N, Puhan S, Nagarajan G, Velappan K. Preparation of palm oil biodiesel and effect of various additives on NO_x emission reduction in B20: An experimental study. *International Journal of Green Energy*. 2011;8(3):383-97.
7. Turrio-Baldassarri L, Battistelli CL, Conti L, Crebelli R, De Berardis B, Iamiceli AL, et al. Emission comparison of urban bus engine fueled with diesel oil and ‘biodiesel’ blend. *Science of the Total Environment*. 2004;327(1-3):147-62.
8. Adu-Mensah D, Mei D, Zuo L, Zhang Q, Wang J. A review on partial hydrogenation of biodiesel and its influence on fuel properties. *Fuel*. 2019;251:660-8.
9. Satterfield CN. *Heterogeneous catalysis in industrial practice*. 1991.
10. Boreskov GK. *Heterogeneous catalysis*: Nova Publishers; 2003.
11. Numwong N, Luengnaruemitchai A, Chollacoop N, Yoshimura Y. Effect of metal type on partial hydrogenation of rapeseed oil-derived FAME. *Journal of the American Oil Chemists' Society*. 2013;90(9):1431-8.
12. Stathis P, Stavroulaki D, Kaika N, Krommyda K, Papadogianakis G. Low trans-isomers formation in the aqueous-phase Pt/TPPTS-catalyzed partial hydrogenation of methyl esters of linseed oil. *Applied Catalysis B: Environmental*. 2017;209:579-90.
13. Quaranta E, Cornacchia D. Partial hydrogenation of a C18: 3-rich FAME mixture

over Pd/C. *Renewable Energy*. 2020.

14. Thunyaratchatanon C, Luengnaruemitchai A, Jitjamnong J, Chollacoop N, Chen S-Y, Yoshimura Y. Influence of Alkaline and Alkaline Earth Metal Promoters on the Catalytic Performance of Pd-M/SiO₂ (M= Na, Ca, or Ba) Catalysts in the Partial Hydrogenation of Soybean Oil-Derived Biodiesel for Oxidative Stability Improvement. *Energy & Fuels*. 2018;32(9):9744-55.

15. Toshima N, Yonezawa T. Bimetallic nanoparticles—novel materials for chemical and physical applications. *New Journal of Chemistry*. 1998;22(11):1179-201.

16. Sinfelt JH. Bimetallic catalysts. *Scientific American*. 1985;253(3):90-101.

17. Edvardsson J, Rautanen P, Littorin A, Larsson M. Deactivation and coke formation on palladium and platinum catalysts in vegetable oil hydrogenation. *Journal of the American Oil Chemists' Society*. 2001;78(3):319-27.

18. Piccolo L, Kibis L. The partial hydrogenation of butadiene over Al₁₃Fe₄: A surface-science study of reaction and deactivation mechanisms. *Journal of Catalysis*. 2015;332:112-8.

19. Brown S. Estimating biomass and biomass change of tropical forests: a primer: Food & Agriculture Org.; 1997.

20. Raveendran K, Ganesh A, Khilar KC. Pyrolysis characteristics of biomass and biomass components. *Fuel*. 1996;75(8):987-98.

21. Vassilev SV, Baxter D, Andersen LK, Vassileva CG, Morgan TJ. An overview of the organic and inorganic phase composition of biomass. *Fuel*. 2012;94:1-33.

22. Chen H. Chemical composition and structure of natural lignocellulose. *Biotechnology of lignocellulose*: Springer; 2014. p. 25-71.

23. Vassilev SV, Baxter D, Andersen LK, Vassileva CG. An overview of the chemical composition of biomass. *Fuel*. 2010;89(5):913-33.

24. Yeo R. Life history of common cattail. *Weeds*. 1964;12(4):284-8.

25. German C, Von Damm K. Hydrothermal processes. *Treatise on geochemistry*. 2006;6:181-222.

26. Byrappa K, Yoshimura M. *Handbook of hydrothermal technology*: William Andrew; 2012.

27. Tekin K, Karagöz S, Bektaş S. A review of hydrothermal biomass processing.

Renewable and sustainable Energy reviews. 2014;40:673-87.

28. Hu B, Wang K, Wu L, Yu SH, Antonietti M, Titirici MM. Engineering carbon materials from the hydrothermal carbonization process of biomass. *Advanced materials*. 2010;22(7):813-28.

29. Kidená K, Murata S, Nomura M. Studies on the chemical structural change during carbonization process. *Energy & Fuels*. 1996;10(3):672-8.

30. Maciá-Agulló J, Moore B, Cazorla-Amorós D, Linares-Solano A. Activation of coal tar pitch carbon fibres: Physical activation vs. chemical activation. *Carbon*. 2004;42(7):1367-70.

31. Sajjadi B, Chen W-Y, Egiebor NO. A comprehensive review on physical activation of biochar for energy and environmental applications. *Reviews in Chemical Engineering*. 2019;35(6):735-76.

32. Sajjadi B, Zubatiuk T, Leszczynska D, Leszczynski J, Chen WY. Chemical activation of biochar for energy and environmental applications: a comprehensive review. *Reviews in Chemical Engineering*. 2019;35(7):777-815.

33. Ma F, Hanna MA. Biodiesel production: a review. *Bioresource technology*. 1999;70(1):1-15.

34. Quitain AT, Katoh S, Goto M. Microwave-assisted synthesis of biofuels. *Biofuel production-recent developments and prospects Rijeka, Croatia: InTech*. 2011:415-36.

35. Hoekman SK, Broch A, Robbins C, Cenicerós E, Natarajan M. Review of biodiesel composition, properties, and specifications. *Renewable and sustainable energy reviews*. 2012;16(1):143-69.

36. Veldsink JW, Bouma MJ, Schöön NH, Beenackers AA. Heterogeneous hydrogenation of vegetable oils: a literature review. *Catalysis Reviews*. 1997;39(3):253-318.

37. Trasarti A, Segobia D, Apesteguía C, Santoro F, Zaccheria F, Ravasio N. Selective hydrogenation of soybean oil on copper catalysts as a tool towards improved bioproducts. *Journal of the American Oil Chemists' Society*. 2012;89(12):2245-52.

38. Winquist BH, Murray BD, Milam SN, Ryan RC, Hastings TW. Hydrogenation catalyst and process. *Google Patents*; 1995.

39. Birch A, Williamson D. Homogeneous hydrogenation catalysts in organic

synthesis. *Organic reactions*. 2004;24:1-186.

40. Argyle MD, Bartholomew CH. Heterogeneous catalyst deactivation and regeneration: a review. *Catalysts*. 2015;5(1):145-269.
41. Yasuda H, Yoshimura Y. Hydrogenation of tetralin over zeolite-supported Pd-Pt catalysts in the presence of dibenzothiophene. *Catalysis Letters*. 1997;46(1-2):43-8.
42. Rane AV, Kanny K, Abitha V, Thomas S. Methods for synthesis of nanoparticles and fabrication of nanocomposites. *Synthesis of inorganic nanomaterials*: Elsevier; 2018. p. 121-39.
43. Brunelle J. Preparation of catalysts by metallic complex adsorption on mineral oxides. *Pure and Applied Chemistry*. 1978;50(9-10):1211-29.
44. Guerreiro E, Gorriz O, Rivarola J, Arrúa L. Characterization of Cu/SiO₂ catalysts prepared by ion exchange for methanol dehydrogenation. *Applied Catalysis A: General*. 1997;165(1-2):259-71.
45. Li G, Hu L, Hill JM. Comparison of reducibility and stability of alumina-supported Ni catalysts prepared by impregnation and co-precipitation. *Applied Catalysis A: General*. 2006;301(1):16-24.
46. Boldrini DE, Tonetto GM, Damiani DE. Experimental study of the deactivation of Pd on anodized aluminum monoliths during the partial hydrogenation of vegetable oil. *Chemical Engineering Journal*. 2015;270:378-84.
47. Rodriguez-Reinoso F, Martin-Martinez JM, Prado-Burguete C, McEnaney B. A standard adsorption isotherm for the characterization of activated carbons. *Journal of Physical Chemistry*. 1987;91(3):515-6.
48. Nishi Y, Inagaki M. Gas adsorption/desorption isotherm for pore structure characterization. *Materials Science and Engineering of Carbon*: Elsevier; 2016. p. 227-47.
49. Jin X-J, Yu Z-M, Wu Y. Preparation of activated carbon from lignin obtained by straw pulping by KOH and K₂CO₃ chemical activation. *Cellulose Chemistry and Technology*. 2012;46(1):79.
50. Abdel-Ghani NT, El-Chaghaby GA, ElGammal MH, Rawash E-SA. Optimizing the preparation conditions of activated carbons from olive cake using KOH activation. *New Carbon Materials*. 2016;31(5):492-500.
51. Namazi AB, Allen DG, Jia CQ. Benefits of microwave heating method in

- production of activated carbon. *The Canadian Journal of Chemical Engineering*. 2016;94(7):1262-8.
52. Rungsi AN, Luengnaruemitchai A, Wongkasemjit S, Chollacoop N, Chen S-Y, Yoshimura Y. Influence of silica sources on structural property and activity of Pd-supported on mesoporous MCM-41 synthesized with an aid of microwave heating for partial hydrogenation of soybean methyl esters. *Applied Catalysis A: General*. 2018;563:80-90.
53. Numwong N, Luengnaruemitchai A, Chollacoop N, Yoshimura Y. Partial hydrogenation of polyunsaturated fatty acid methyl esters over Pd/activated carbon: Effect of type of reactor. *Chemical engineering journal*. 2012;210:173-81.
54. Numwong N, Luengnaruemitchai A, Chollacoop N, Yoshimura Y. Effect of support acidic properties on sulfur tolerance of Pd catalysts for partial hydrogenation of rapeseed oil-derived FAME. *Journal of the American Oil Chemists' Society*. 2012;89(11):2117-20.
55. Jitjamnong J, Niseng S, Khantikulanon N, Samanwong N. Catalytic Activity of Ni/SiO₂ Supported on Partial Hydrogenation of Biodiesel from Waste Cooking Oil. *Thaksin University Journal*. 2018;21(3):99-106.
56. Thunyaratchatanon C, Luengnaruemitchai A, Chollacoop N, Yoshimura Y. Catalytic upgrading of soybean oil methyl esters by partial hydrogenation using Pd catalysts. *Fuel*. 2016;163:8-16.
57. Wei G, Liu Z, Zhang L, Li Z. Catalytic upgrading of Jatropha oil biodiesel by partial hydrogenation using Raney-Ni as catalyst under microwave heating. *Energy Conversion and Management*. 2018;163:208-18.
58. Thunyaratchatanon C, Jitjamnong J, Luengnaruemitchai A, Numwong N, Chollacoop N, Yoshimura Y. Influence of Mg modifier on cis-trans selectivity in partial hydrogenation of biodiesel using different metal types. *Applied Catalysis A: General*. 2016;520:170-7.
59. McArdle S, Leahy JJ, Curtin T, Tanner D. Hydrogenation of sunflower oil over Pt-Ni bimetallic supported catalysts: preparation, characterization and catalytic activity. *Applied Catalysis A: General*. 2014;474:78-86.
60. Zhao Y, Ren Y, Zhang R, Zhang L, Yu D, Jiang L, et al. Preparation of

hydrogenated soybean oil of high oleic oil with supported catalysts. *Food bioscience*. 2018;22:91-8.

61. Li S, Han K, Li J, Li M, Lu C. Preparation and characterization of super activated carbon produced from gulfweed by KOH activation. *Microporous and Mesoporous Materials*. 2017;243:291-300.

62. Jaruwat D, Udomsap P, Chollacoop N, Fuji M, Eiad-ua A, editors. Effects of hydrothermal temperature and time of hydrochar from Cattail leaves. *AIP Conference Proceedings*; 2018: AIP Publishing LLC.

63. Yao Z, Ma X, Wu Z, Yao T. TGA-FTIR analysis of co-pyrolysis characteristics of hydrochar and paper sludge. *Journal of Analytical and Applied Pyrolysis*. 2017;123:40-8.

64. Tseng R-L, Tseng S-K, Wu F-C, Hu C-C, Wang C-C. Effects of micropore development on the physicochemical properties of KOH-activated carbons. *Journal of the Chinese Institute of Chemical Engineers*. 2008;39(1):37-47.

65. Dizbay-Onat M, Vaidya UK, Lungu CT. Preparation of industrial sisal fiber waste derived activated carbon by chemical activation and effects of carbonization parameters on surface characteristics. *Industrial crops and products*. 2017;95:583-90.

66. Manoj B, Kunjomana A. Study of stacking structure of amorphous carbon by X-ray diffraction technique. *Int J Electrochem Sci*. 2012;7(4):3127-34.

67. Xiang X, Liu E, Li L, Yang Y, Shen H, Huang Z, et al. Activated carbon prepared from polyaniline base by K_2CO_3 activation for application in supercapacitor electrodes. *Journal of Solid State Electrochemistry*. 2011;15(3):579-85.

68. Puna J, Gomes J, Correia MJN, Dias AS, Bordado J. Advances on the development of novel heterogeneous catalysts for transesterification of triglycerides in biodiesel. *Fuel*. 2010;89(11):3602-6.

69. Udomsap P, Meesiri S, Chollacoop N, Eiad-Ua A. Biomass Nanoporous Carbon-Supported Pd Catalysts for Partial Hydrogenation of Biodiesel: Effects of Surface Chemistry on Pd Particle Size and Catalytic Performance. *Nanomaterials*. 2021;11(6):1431.

70. Naderi M. *Surface Area: Brunauer-Emmett-Teller (BET)*. *Progress in filtration and separation*: Elsevier; 2015. p. 585-608.

71. Lee AF, Wilson K. Recent developments in heterogeneous catalysis for the

sustainable production of biodiesel. *Catalysis Today*. 2015;242:3-18.

72. Kan Y, Yue Q, Li D, Wu Y, Gao B. Preparation and characterization of activated carbons from waste tea by H₃PO₄ activation in different atmospheres for oxytetracycline removal. *Journal of the Taiwan Institute of Chemical Engineers*. 2017;71:494-500.

73. Gao G, Shao Y, Gao Y, Wei T, Gao G, Zhang S, et al. Synergetic effects of hydrogenation and acidic sites in phosphorus-modified nickel catalysts for the selective conversion of furfural to cyclopentanone. *Catalysis Science & Technology*. 2021;11(2):575-93.

74. Gupta D, Kumar R, Pant KK. Hydrotalcite supported bimetallic (Ni-Cu) catalyst: A smart choice for one-pot conversion of biomass-derived platform chemicals to hydrogenated biofuels. *Fuel*. 2020;277:118111.

75. Chen B, Li F, Huang Z, Yuan G. Carbon-coated Cu-Co bimetallic nanoparticles as selective and recyclable catalysts for production of biofuel 2, 5-dimethylfuran. *Applied Catalysis B: Environmental*. 2017;200:192-9.

76. Yusoff MNAM, Zulkifli NWM, Sukiman NL, Chyuan OH, Hassan MH, Hasnul MH, et al. Sustainability of palm biodiesel in transportation: a review on biofuel standard, policy and international collaboration between Malaysia and Colombia. *Bioenergy research*. 2021;14(1):43-60.

77. Irandoust S, Edvardsson J. Poisoning of nickel-based catalysts in fat hydrogenation. *Journal of the American Oil Chemists Society*. 1993;70(11):1149-56.

78. Zufarov O, Schmidt Š, Sekretár S. Degumming of rapeseed and sunflower oils. *Acta Chimica Slovaca*. 2008;1(1):321-8.



จุฬาลงกรณ์มหาวิทยาลัย
CHULALONGKORN UNIVERSITY

VITA

NAME Tripob Longprang

DATE OF BIRTH 14 Jan 1997

PLACE OF BIRTH Bangkok

INSTITUTIONS ATTENDED Bachelor of Nanomaterial Engineering

HOME ADDRESS 53/18 Moo. 5, Hua ro, Phra Nakhon Si Ayutthaya, Phra Nakhon Si Ayutthaya 13000

PUBLICATION

[1] Tripob Longprang, Dolrudee Jaruwat, Buachum Udomsap, Nuwong Chollacoop and Apiluck Eiad-ua, Influence of Acid Additive on Nanoporous Carbon Materials via HTC for Catalyst Support, Materials Today Proceeding.

[2] Tripob Longprang, Dolrudee Jaruwat, Parncheewa Udomsap, Nuwong Chollacoop, Apiluck Eiad-ua, Influence of Base Additive on Nanoporous Carbon Materials via HTC for Catalyst Support, International Journal of Science and Mathematic Education.

[3] Tripob Longprang, Parncheewa Udomsap, Nuwong Chollacoop, Masayoshi Fuji and Apiluck Eiad-ua, Preparation of Monometallic Catalysts on Carbon Support for Synthesis of Biodiesel Fuel, Key Engineering Materials.

[4] Tripob Longprang, Apiluck Eiad-ua, Nuwong Chollacoop, Worapon Kiatkittipong, Atthapon Srifa and Suttichai Assabumrungrat, Monometallic and Bimetallic Catalysts on Nanoporous Carbon Support for Synthesis of Partially Hydrogenated Fatty Acid Methyl Ester (H-FAME), International Conference on Engineering, Applied Sciences and Technology Proceeding



จุฬาลงกรณ์มหาวิทยาลัย
CHULALONGKORN UNIVERSITY